TAMPEREEN TEKNILLINEN YLIOPISTO
TAMPERE UNIVERSITY OF TECHNOLOGY

HAIDER IFTIKHAR

TRANSPARENT INDIUM TIN OXIDE MICROELECTRODE ARRAYS FOR MEASURING BEATING CARDIOMYOCYTES

Master of Science Thesis

Examiners:

Professor Jukka Lekkala
MSc. Tomi Ryynänen

Examiners and topic approved at the council meeting of Faculty of Natural Sciences on 30th May 2015

ABSTRACT

Tampere University of Technology
International Master's degree in Science & Bioengineering
Haider Iftikhar: Transparent Indium Tin Oxide Microelectrode Arrays for Measuring Beating Cardiomyocytes
Master of Science Thesis, 81 pages, 3 Appendix pages
December 2016
Major: Biomeasurements
Examiners: Professor Jukka Lekkala and MSc. Tomi Ryynänen

Keywords: MEA, ITO, Cardiomyocyte, Microfabrication, EB-PVD, RIE

This thesis study was made, to develop the microfabrication process for transparent microelectrode arrays (MEAs) using indium tin oxide (ITO). This was done in order to measure bioelectrical data from cardiomyocytes (CMs), without owing any obscurities due to electrodes, as it happens in the conventional MEAs. The study was carried out in three tier (parts) fashion, wherein the 1st tier was dedicated in development of transparent ITO films. The 2nd tier involved with, the transparent ITO films that were developed in the 1st tier, to be patterned into microstructures present in the MEAs. The 3rd and the final tier dealt with two important tasks. The first including, optimizations needed in the previous two tiers, in order to come up with a viable microfabrication process to develop transparent ITO MEAs. The second task of the 3rd tier covered all the necessary testing required to ensure for the best possible quality of measurements of the bioelectric signals. The study showed that the ITO layers developed had very good transparencies of more than 90% transmissions possible, with sheet resistances in the range of 13-46 Ω/sq. The results from cell experiments showed that the MEAs not only measured electrical signals of cardiomyocytes aggregates but also owed no obscurities via microscopes, in the process. The electrode impedance measurements showed that the electrodes were comparable with commercially available ITO MEAs with mean values of 1200 kΩ. The measurements of noise levels were measured in reference to a commercial titanium nitride (TiN) MEA and the noise levels were comparable. Data from other literature studies was compared to ITO electrodes from this study to theirs, it was discovered that noise levels from this study were much better than their ITO electrodes and even certain gold (Au) electrodes.

The process for ITO layer deposition was done using electron beam physical vapour deposition (EB-PVD), and later the annealing was made at temperatures from 300-500 °C. The MEA microfabrication of the ITO layers was done, by dry etching the ITO layers using reactive ion etching (RIE) device through argon. The insulation layer of silicon nitride was deposited using plasma enhanced chemical vapour deposition (PECVD) process by the personnel at the Optoelectronic Research Centre (ORC) of Tampere University of Technology. The insulation layer was also patterned using dry etching, by the same device. The beating cardiomyocyte and noise measurements were done at BioMediTech.

PREFACE

In the name of ALLAAH, Most Gracious Most Merciful

This thesis is the monumental part of my Master's study at the TUT, as it was done under the guidance of highly skilled professionals aiming to improve quality of life as a service to mankind and nature. This thesis serves as rudimentary step in this great mission. The documentation of my research during the eventful study is a record of all the eventful and uneventful misgivings occurring in the research as well. It presents the results of a study towards the microfabrication of MEAs from ITO to facilitate biologists in the simultaneous unhindered viewing of the cardiomyocytes while recording signals *in-vitro.* It specifically focuses on most challenges faced in microfabrication and provides an insight for the practical implementation of all theoretical steps required to fabricate MEAs in house from stretch. The study had its labours undoubtedly but the opportunity to work with extremely sophisticated machines like a Metallization device, Reactive Ion Etching device, and the opportunity of working in a Cleanroom, made all the hard work worth the while.

The most fun part was the learning experience with Mr Tomi Ryynänen who also happened to be my supervisor and one of the examiners of my thesis. He not only taught me what I know as a researcher but also befriended me. I drove all my inspiration form Professor Jukka Lekkala, the other examiner, since he pushed me to complete my writing for this thesis which seemed impossible at times. I am sincerely thankful to Mr Joose Kreutzer for graciously providing the PDMS rings for my ITO MEAs. I would also like to extend my reverence to Professor Katriina Aalto-Setälä and her group at the Univeristy of Tampere, for making the cardiomyocyte measurements with the MEAs I fabricated. I am most indebted to Mr. Disheet Shah at BioMediTech who put tireless efforts, to culture cardiomyocytes for the experimentation over period of days, and became a very good friend as well. I would also take a moment to thank Ms Mervi Koskinen at the ORC for depositing the silicon nitride insulation layer and help provide most of the photographs used in this document. Special regards for Miss Suvi Heinamäki who provided me access to the furnace for annealing my ITO layers. My wife deserves my absolute gratitude and appreciation who kept me motivated for writing of this thesis by not only cooking my favourite cuisines but also helping me in the writing process. I would extend my profound acknowledgement and gratefulness to my parents and friends who believed in me and supported me in this time of great hardship. Finally, I would thank ALLAAH subhana wa taa'la for granting me the courage and perseverance and ability to complete this study.

Tampere, 24.11.2016

Haider Iftikhar

CONTENTS

LIST OF FIGURES

LIST OF TABLES

LIST OF SYMBOLS AND ABBREVIATIONS

ADC	Analog to Digital Convertor
AFM	Atomic Force Microscope
ASCII	American standard code for information interchange
Au	Gold
AZO	Aluminum zinc oxide
bpm	Beats per minute
℃	Degree Celsius
Cl	Chloride ion
CM	Cardiomyocyte
CMOS	Complementary metal–oxide–semiconductor
CPU	Central processing unit
CVD-	Chemical vapour deposition
DI	De ionized
DMM	Digital multi meter
EB-PVD	Electron Beam Physical Vapour Deposition
Eg(eV)	Band gap energy in electron volts
EMI	Electromagnetic
FBS	Foetal Bovine Serum
FTO	Fluorine-doped Tin Oxide
H^+	Hydrogen ion
H_2O	Water
H_2O_2	Hydrogen per oxide
HCl	Hydrochloric acid
HD	High Density
HF	Hydrofluoric acid
HMDS	Hexamethyldisilazane
HNO_3	Nitric acid
I/O	Input/ Output
IAD	Ion assisted deposition
IBAD	Ion beam assisted deposition
In	Indium
IPA	Isopropanol
Ir	Iridium
IR	Infrared
ITO	Indium Tin Oxide (In_2O_3 +SnO_2)
LCD	Liquid Crystal Display
LTD	Long term depression
LTP	Long term potentiation
MCS	Multi Channel System
MEA	Microelectrode Array
MEA-IT	Microelectrode array impedance testier
NIR	Near Infrared
ORC	Optoelectronics Research Centre
PBS	Phosphate- Buffered Saline
PC	Personal Computer
PDMS	Polydimethylsiloxane
PECVD	Plasma Enhanced Chemical Vapour Deposition

PET	Polyethylene terephthalate
PPF	Paired Pulse Facilitation
Pt	Platinum
PVD	Physical vapour deposition
RCA clean	Standard set of wafer cleaning steps developed by Radio Corporation of America
RF	Radio Frequency
RIE	Reactive Ion Etching
R_s	Sheet Resistance
SEM	Scanning Electron Microscope
Si_3N_4	Silicon nitride
Sn	Tin
SnO_2	Tin oxide
TCF	Thin conductive film
TCO	Transparent conducting oxide
TH	Tungsten Halogen
Ti	Titanium
TiN	Titanium nitride
TUT	Tampere University of Technology
USB	Universal Serial Bus
UTA	University of Tampere
Vis-NIR	Visible to Near Infrared
XRD	X-Ray Diffraction
μEEG	Micro electroencephalogram
μERG	Micro-electroretinogram

1. INTRODUCTION

There has been a lot of focus on the study of different type of cells within the human body to gather a more updated knowledge of the proper functioning of different organs of the body. In recent studies it has been discovered that a cluster of cells working together have an altogether different behaviour compared to an individual cell of the same specie [1]. One of the ways to study cells individually has been through the help of patch clamp technique; where the electrical data acquired is related to the physiological activity of a particular cell. This signifies that there exists a meaningful relation between the electrical activities of the ionic pumps within the cells to actual cellular activity within their extra cellular matrix.

Though the patch clamp technique offers quite reliable data, it does so while destroying the cell in the process or at the very least causing the cell to be under high stress, which causes skewing of certain data points. In order to study cells in their residual state there was a requirement for less intrusive methods and therefore it paved way for Microelectrode Arrays (MEAs), which became a more suitable alternative while being less intrusive and disruptive. Although MEAs seem as a better choice for cell study analysis, they still need to be customized and tailored to acquire the necessary data without huge losses, irregularities and drawbacks. Simply put, MEAs can be tailored uniquely according to their use of application each time.

One of the most critical drawbacks in the conventional MEAs is that the cells often get obscured by the opaque electrodes under the light microscopes, while still being recorded. This causes blockage in observatory field necessary to relate electrical data to the physical changes of the cells. “Invention is the mother of necessity”, so this research study was dedicated to address the challenge of fabricating customized MEAs that could measure the electrical data without causing the obscurity of the cells under the microscope. Thus, the main goal of this study was to develop in house customized MEAs that could both, measure the electrical activity of beating Cardiomyocytes (CM) while facilitating visual recording of the concurrent physiological changes without any visual obstruction owing to the electrode opacity.

Commercially available conventional MEAs are fabricated using metals or highly conductive compounds, usually which are opaque in nature, thus obscuring certain parts of the cells when studied under optical microscopes. The exclusive requirement for transparency in electrodes led the study to search for transparent compounds which also needed to be decent conductors. Such conductors would also be required to be deposited as thin conductive films (TCFs). Amongst all the TCFs the most suitable candidate

known due to its immense popularity was Indium Tin Oxide (ITO), and was thus chosen as the target material. ITO was already well known for its innate properties of low sheet resistance, high conductivity and high transparency. These properties had already earned huge commercial success for its application in touch screen technology for front panel displays and touch screen displays of mobiles and tablet PCs. The other, more important, reason for ITO's selection was its feasibility of deposition over glass substrate, which is possible by a number of processes. However, its possible deposition with the facility available at our own department, the Electron Beam Physical Vapour Deposition (EB-PVD) device, was also a deciding factor.

Apart from ITO being a wondrous material for providing transparency along with conduction, it was found to be conveniently biocompatible as well. Of course when studying CMs and that too in viable beating state, it is imperative that the material used for electrodes be inert and has neither degradative nor toxic effect over the cells intended to be studied. Therefore, while considering for ITO as the material of choice, its biocompatibility was also researched and found to be comparable of that of gold. The biocompatibility of ITO is more thoroughly discussed in the following topics to come. Since ITO was an exceptional material that fulfilled all the requirements to fabricate the kind of electrodes required for this study and EB-PVD was the most convenient choice for deposition, therefore not a lot of study was required to figure out alternative methods for deposition and neither for materials alternative to ITO in general.

Even though the choices were predetermined, the execution of the study required recursive experiments to figure out if the combination of the two were adequate for this study. The deposition process of ITO with EB-PVD needs to be very precise in order to deposit a thin film for optimal optical transmission as well as for electrical conduction. Earlier results from the studies of ITO thin film deposition also helped confirm that EB-PVD was fortunately a good choice for deposition as it is expected to be both, highly economic and highly robust deposition technique at the same time [2]. EB-PVD is a robust method that allows higher efficiency of material utilization compared to other methods. It also has a decent variation for both low and high deposition rates, and since it can support high deposition rates it has a lot of industrial application that relates to it [2].

The thesis study was carried out in three tiers or phases and is therefore written accordingly. The first tier of the study was, to be able to develop transparent thin films of ITO which had low sheet resistances and good conduction. It was made possible with the right combinations of the deposition rate and post annealing temperatures of the films. Where EB-PVD is a suitable method to develop ITO thin film, it is still not commercially conventional or the optimal method that develops transparent and conductive films right away. Therefore, choosing the right deposition rate and post deposition annealing were required, to render the post deposited film of ITO to be both transparent and conductive. Researching the right deposition rate was the most important challenge as it is

the key component that determines the quality of the film. Temperature for annealing was another integral part in the first tier and is discussed in more detail in the experimentation part.

The second tier of the study included the fabrication of MEA patterns out of the ITO thin films over glass substrates, to be finalized into a MEA configuration. The main challenge of the second tier involved exhaustive experimentations of both wet and dry etching processes for microfabrication of the ITO thin film into MEAs, which too was successful eventually. Etching ITO on glass was the most difficult and time consuming part of the study other than writing the thesis. It was learnt, that wet etching would not work for this study. Plasma etching was necessary for maintaining the structural integrity of the required MEA pattern in the micrometre dimensions.

The third tier included challenges involving, the testing and making measurements to see if the prototypes were functional and able to achieve the set goal, which too was successful. There were optimizations and customizations needed to come up with the best results, and is discussed in detail in the upcoming topics.

2. ELECTRON BEAM PHYSICAL VAPOR DEPOSITION

2.1 Introduction

Electron beam physical vapour deposition (EB-PVD) is a variant method of physical vapour deposition, where an electron beam is generated by heating a tungsten filament under high vacuum, to convert atoms of target material at anode into vapours that can then be used to coat a substrate.

EB-PVD's exclusive application in microfabrication processes involves thin film deposition, a process un-foreign to the semiconductor industry, where it utilized to grow electronic materials. It is employed in forming thermal and chemical barrier coatings in the aerospace industry, to protect surfaces against corrosive environments. In the field of optics its application brings forth desired reflective and transmissivity properties to a substrate and elsewhere in the industry, EB-PVD modifies surfaces to achieve a variety of desired properties.

2.2 Deposition Processes

When it comes to deposition process, it can be generally classified into physical vapour deposition (PVD), chemical vapour deposition (CVD) and spray processes [3]. Each process has further sub-classifications based on the source of energy used for the deposition of coatings as illustrated in Table 1. Each of the mentioned processes has its own advantages and disadvantages. The parameters of the deposited material such as the composition, residual stresses, and microstructure (e.g. being amorphous, polycrystalline, epitaxial, and textured etc.) are all strongly affected by the chemical and physical conditions during the deposition reaction. The precise process control for any deposition requires the exact knowledge and effect of these conditions. Thus, the application of the final product, coating thickness and other desired properties such as microstructure, physical, and mechanical properties are the determinant of the coating process to be used.

Table 1. *Different categories and classifications of deposition processes*

Chemical Vapor Deposition Processes (CVD)
Low pressure CVD
Plasma enhanced CVD
Photochemical and laser-CVD
Physical Vapor Deposition Processes (PVD)
Thermal evaporation
Electron beam evaporation
S p u t t e r i n g
-Balanced and unbalanced magnetron sputtering
-Direct current diode sputtering
-Radio frequency sputtering
-Triode-assisted PVD
Ion plating and ion implantation

2.2.1 Chemical Vapour Deposition

The process of chemical vapour deposition (CVD) makes use of a reactant gas mixture which when passed through a high-temperature reactor can form a solid product in the form of a thin film on the surface of the substrate. The CVD coating process requires operational temperatures in the range of 800 and 1200 °C. As an advantage CVD process provides dense, homogeneous and high quality films. These films can be of various metallic and ceramic coatings (like oxides, carbides, and nitrides) which are able to be deposited. The most obvious disadvantage of the CVD process include the often requirement of high deposition temperatures which can be addressed by one of its variant, Plasma Enhanced Chemical Vapour Deposition (PECVD), which was also utilized in this study [3].

PECVD is mainly used to deposit dielectric and/or passivation films like silicon oxide and nitride at low temperature. Unlike PVD, the necessary energy for the chemical reaction is not introduced by heating, instead the whole reaction chamber is filled with heated gas or plasma. An RF generator is used to generate the plasma required in the reaction chamber which also contains reactive ions and radicals. The intense bombardment of the ion from the plasma on the substrate gives a good initial growth due to cleaning of the surface. This eventually provides good adhesion and high growth rates as the process progresses. The coated layers can be better influenced for their properties with PECVD, since more process parameters can be varied in comparison to thermal deposition technique. Adjustment of adhesion, compressive and tensile stress causing warpage, hydrogen content and density, etchability, etch rate and selectivity in etching, step coverage as well as stoichiometry (consistence) and cleanliness of the deposited layers, which can be measured by the refractive index, are all important for PECVD process [3].

.

2.2.2 Physical Vapour Deposition

The term physical vapour deposition (PVD) refers to those vacuum deposition processes wherein the coating material is made to evaporate by various mechanisms (resistance heating, high-energy ionized gas bombardment, or electron gun) under vacuum. The resulting vapour phase is directed on to the substrate, resulting into a thin coating formed atom by atom or molecule by molecule. PVD is a process in which atoms/molecules travel to the substrate from the source material in a straight path and therefore is termed as a line-of-sight process. The PVD coating process can take place at temperature up to 3500 °C. Amongst all the PVD processes sputtering is considered one of the most versatile processes available for thin film preparation. Most metallic and various ceramic coatings are able to be deposited using this process, typically at a rate of a few um or less per hour [3]. Some of the shortcomings of the CVD process are addressed by the PVD process. Unlike the CVD process, PVD processes are clean and pollution free, unless the users contaminates the source material, substrates or the vacuum chamber. The main disadvantages of PVD processes include low deposition rates and the difficulty in applying oxide coatings efficiently (with exception of EB-PVD which have higher deposition rates and broader variety of materials to deposit compared to rest of PVD processes) [3].

Even though PVD processes have advanced variants, however non-homogeneity in the microstructure prevails, which is detrimental to the physical properties of the deposited film. In sputtering processes, plasma of inert gas ions is produced by applying an electric field. These ions can then strike the cathode composed of the target material, upon striking, the ions knock out atoms from the cathode. The ejected atoms from the target material are finally deposited on the surface of the substrate. The disadvantage in this case so happens to be, that sometimes the target atoms can also combine with reactive gases just before deposition to form unwanted ceramic coatings [3]. The disadvantage of the above mentioned PVD process can be addressed by the EB-PVD.

2.3 EB-PVD Phenomenon and Theory

The EB-PVD process has the ability to overcome some of the difficulties associated with other deposition processes and is a better variant of PVD for high quality, resilient, and robust coatings. Deposition by EB-PVD process focuses high energy electron beams generated from electron guns, which are channelled to melt and evaporate ingots or target materials in crucibles. There is also possibility of preheating the substrate inside the vacuum chamber during the deposition process. The vacuum chamber can also be referred to as the deposition chamber, and requires to be depressurized to at least 7.5 x 10^{-5} Torr (10^{-2} Pa) to ensure unhindered emission of electrons from the electron gun. This beam of emitted electrons causes the evaporation of the target material which can be in the form of an ingot or rod [1]. In some modern EB-PVD systems an arc suppres-

sion system is incorporated and can help operate at lower vacuum levels of 5.0 x 10^{-3} Torr. This gives the process a leg up and facilitates parallel use of magnetron sputtering alongside [2]. The diversity of EB-PVD is that it can accommodate multiple types of evaporation materials and multiple electron guns simultaneously, each ranging from tens to hundreds of kW in power. The electron beams used to melt or sublimate the target material are generated by either, thermionic emission, field electron emission or the anodic arc method. In either case, the electron beam generated is then accelerated to a high enough kinetic energy as well as directed towards the evaporation material using electrostatic mechanism. Once the beam is directed to the target material, the electrons in the beam begin striking the evaporation material, causing the electrons to lose their energy to the target material. The kinetic energy of the electrons is converted into other forms; amongst them the thermal energy produced heats up the target material causing it either to melt or to sublimate. The resulting vapour from the melted or sublimated target at the appropriate temperature and pressure is then used to coat surfaces. The accelerating voltages are vital to the process and can vary between 3 kV – 40 kV. However, for optimum conversion of the electron's kinetic energy into thermal energy of the target material the accelerating voltage is maintained between 20 kV – 25 kV and the beam current is a few amperes. This results in an efficiency of 85 % conversion of the electron's kinetic energy into thermal energy. The 15 % deficit in the conversion efficiency is due to the incident electron energy lost through the production of X-rays and secondary electron emissions.

EB-PVD exists in three configurations, electromagnetic alignment, electromagnetic focusing and the pendant drop configuration, when it comes to evaporation material utilization. In the electromagnetic alignment and electromagnetic focusing configurations the evaporation material is utilized in the form of an ingot. However, the pendant drop configuration utilizes a rod. Ingots are usually enclosed in a (copper or a graphite) crucible or hearth, a rod on the other hand is usually mounted at one end in a socket more or less. The crucible and socket both require cooling which is typically aided by water circulation. Molten liquid can form on the surface of an ingot when metals are being used, which can be kept constant by vertical displacement of the ingot. In which case, evaporation rates may be on the order of 10^{-2} g/cm^2 sec.

2.3.1 Material Evaporation Behaviour

Evaporation of different materials with EB-PVD is not always similar. Certain carbides especially refractory carbides like titanium carbide and borides like titanium boride and zirconium boride can evaporate without undergoing decomposition in the vapour phase. Thus direct deposition by simple evaporation for such compounds is possible, in form of compacted ingots. These compounds get evaporated in vacuum by focused high energy electron beam, causing direct condensation of vapours directly over the substrate.

Alternatively certain refractory oxides and carbides fragment, while evaporating in the process, causing in a stoichiometry of material over the substrate that is different from the initial material. For example, In_2O_3, SnO_2, InO, InO_2 and SnO are formed during the evaporation process during the EB-PVD when ITO is focused with the e-beam. Similarly, some refractory carbides for instance, silicon carbide and tungsten carbide, upon heating decompose resulting in dissociated elements that have different volatilities. Such compounds need to be deposited over the substrate either by reactive evaporation or by co-evaporation. The reactive evaporation process differs from conventional e-beam, wherein the metal evaporated from the ingot by the electron beam is carried by the reactive gas, which is oxygen in case of metal oxides and acetylene in case of metal carbides. The film deposits in the proper stoichiometry, as a result of thermodynamic reaction between the vapour and the gas in the vicinity of the substrate.

2.4 Advantages & Disadvantages

2.4.1 Advantages

The main advantages of EB-PVD process in thin film deposition include possibilities for controlling variations in the structure and composition of the condensed materials. For example, coatings comprised of alternating layers of different compositions can be made. Also, it offers many desirable characteristics such as relatively high deposition rates, dense coatings, controlled composition control and microstructure, low contamination, and high thermal efficiency. The coatings produced by the EB-PVD process usually have a good surface finish and a uniform microstructure, which is the most integral reason in thin film deposition such as ITO. The microstructure and composition of the coating can be easily maintained or altered by manipulating the process parameters and ingot compositions. Materials with low vapour pressure can readily evaporated by this process. Thus, coatings such as ITO layers can be readily formed at relatively low temperatures with lower deposition rates. Though they are amorphous, nonconductive and opaque but that can also be treated [3-4].

With the attachment of an ion beam source to the EB-PVD system, additional benefits such as forming dense coatings with improved microstructure, interfaces, and adhesion, can be attained as well. In addition, textured coatings can also be obtained that are desirable in many applications in microfabrication e.g. surfaces with nano-pillar etc. A high-energy ion beam (as a source of energy) is quite often used to clean the surface of the specimen inside the vacuum chamber prior to coating. The cleaning enhances the bonding strength between the coating and the substrate. In case of ITO transparent conductive coatings can be deposited at room temperature with the use of ion beams incorporated to EB-PVD process without post annealing [4].

2.4.2 Disadvantages

When performed at low pressures (< 10^{-4} Torr), EB-PVD strictly behaves as a line-of-sight deposition process. The translational and rotational motion of the shaft helps for coating the outer surface of complex geometries, but this process cannot be used to coat the inner surface of complex geometries. However at higher pressures the inner surface of the complex geometries can be coated. Another potential problem is that filament degradation in the electron gun results in a non-uniform evaporation rate and high radiant heat loads can also exist in the deposition system [4].

3. INDIUM TIN OXIDE (ITO)

3.1 General Properties

In the field of thin conducting films (TCFs) and transparent conducting oxides (TCOs) Indium tin oxide (ITO) enjoys the "gold standard", it is the most widely used and manufactured of the TCOs for the application of TCFs [5]. Besides having numerous applications as thin films, the most common applications of ITO include transparent electrodes for a range of display, photovoltaic and sensor applications for solar cells and panels, EMI shielding, low e-windows, transparent heaters, and famously for transparent electronics. When considering TCOs or TCFs, they are supposed to comprise of a combination of good visible transmittance and electrical conduction, amongst all ITO generally leads the way. High quality ITO can have a resistivity as low as $2x10^{-4}$ Ωcm compared to silver's $1.8x10^{-6}$ Ωcm, electrical properties depended on carrier density [5].

3.1.1 Compositions

ITO is basically considered as indium (III) oxide In_2O_3 doped with tin (IV) oxide SnO_2, a mixture of In_2O_3 and SnO_2. Typically In_2O_3 ranges from 95 % to 80 % and SnO_2 ranges from 5 % to 20 % by weight in the composition of the film, according to its application and usage [5-6]. In_2O_3 fundamentally is an n-type semiconductor material, it is transparent and colourless in thin layers while in bulk form it appears to be yellowish to grey. It acts as a metal-like mirror when exposed in infrared regions of light [6].

As the major two properties of the ITO for which it is famous for that are its conductivity and its transparency, the factors that improve these characteristics need to be understood. Amongst all the factors that affect the transparency without decreasing the conductivity is the ratio of In to Sn. The tested and optimized percentage weight of Sn in the mixture is actually found out to be 20 %, at which the electron mobility, resistivity and visible transmittance all are optimized [5]. Below this percentage, the electrical properties are determined basically through doping concentration as well as scattering off oxygen vacancies for higher levels of Sn. At this doping level, the internal transmittance is 91 %, which does not include the transmittance of the substrate and the mobility is 40 cm^2/Vs. Figure 3.1 better elaborates the dependency of the Sn levels to the mentioned three properties [5].

3.1.2 Optical Properties

The refractive index and extinction coefficient of ITO depends largely on the deposition process, the amount of Sn content, and oxygen vacancies, and no one set of n and k values can represent all films. However, in general, the refractive index is found to lie in the range of 1.8 – 1.9 for most films and the extinction coefficient for transmissions of ITO is less than 0.01 at visible wavelengths [5]. Figure 3.2, elaborates the dependence of transmittance on resistivity, where it exhibits a metal-like behaviour with decreased resistivity. These spectra demonstrate that conductive films with excellent visible transmittance can be deposited, but visible transmittance generally decreases and NIR – IR reflectance increases with decreasing resistivity, as predicted by Drude model. Finally, good ITO is completely clear. If too much Sn is added the films become tan and dark, and the films turn pale green and yellow as scattering from oxygen vacancies increases.

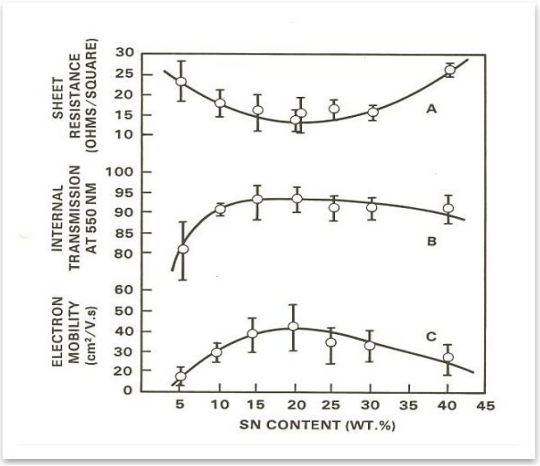

Figure 3.1: *Dependence of sheet resistance (A), visible transmittance (B), and electron mobility (C) on Sn content for magnetron sputtered ITO [5].*

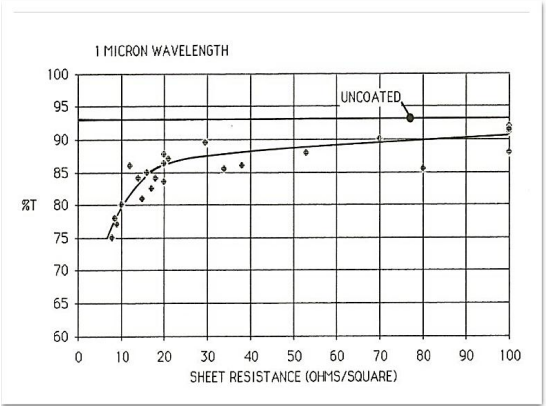

Figure 3.2: *Dependence of the transmittance of magnetron sputtered ITO at 1000 nm wavelength on sheet resistance [5].*

3.1.3 Electrical Properties

Since the resistivity of the films depends on electron conduction, defects and grain boundaries, thus the goal of the deposition processes is to produce films with the largest possible grain size. Having a larger grain size also causes an increase in the Hall mobility. This can be accomplished by heating the substrate during the process of deposition [7]. Films are often heat treated after deposition. Post deposition heat treatment is generally not an option for films on plastic substrates.

ITO when deposited as thin film can be extremely tricky as it follows a “Goldilock’s principle” where all the parameters have to be just right during the deposition process and during the post deposition process as well. The reason is because the composition of the ITO varies in both the deposition and at the time of annealing. During deposition the ITO tends to sublimate rather than melting down first conventionally, in doing so it also disintegrates into sub molecular species. The disintegration tends to be higher at higher deposition rates and significantly less at lower deposition rate. During annealing the oxygen scattering off for higher Sn levels can change causing more oxygen to be adsorbed in the film. The variation of the ITO’s composition to its electro-optical properties can be better understood by the illustration in Figure 3.3.

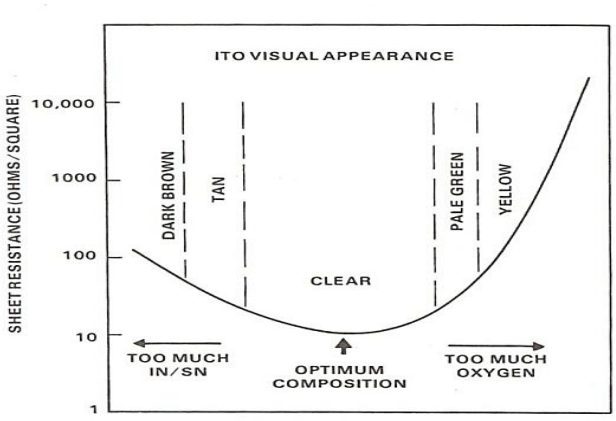

Figure 3.3: *Resistivity well of ITO owing to its physical composition on In, Sn and O [5].*

3.2 ITO Film Deposition

Thin films of indium tin oxide are deposited by various techniques of PVD; amongst them most common are Magnetron sputtering and RF sputtering. However, the later are more famous commercially, EB-PVD has also been used quite extensively for deposition of ITO, especially in the fields of academic research [8-10, 19]. As already mentioned in Chapter 2, the main focus revolves around EB-PVD due to its availability, thus the intention of discussing the parameters involving ITO deposition by EB-PVD.

From the economical point of view, obtaining ITO films with low resistivity and high visible transparency produced at a significantly lower substrate temperature during the deposition process is very important and thus the reason of choice as well [8]. Low substrate temperature depositions do not require a substrate heater to be installed in the metallization device, these are costly to install and they consume higher energy than otherwise already high energy consuming depositions. Though the electron beam evaporation is not a conventional technique to deposit ITO films, it was another research innovation to explore the possibilities of deposition by this method.

3.2.1 Substrate Considerations

When depositing ITO a few things need to be taken into account, prior to deposition. The first and the foremost parameter to consider, is to understand what substrate is going to be used for deposition. The substrates can range from glass, metal, semiconductors and even polymers. The method of deposition for each substrate type, though is more or less the same in each deposition methodology varying slightly for plastics and polymers substrates, however the pre-treatment and post-treatment of the substrate to the deposition can vastly differ. One example that can give a better understanding of the point in discussion is, when solely ITO is deposited at room temperature without any ion source or ion assisted deposition, the ITO layer is dark and opaque [8]. This dark and opaque layer is also high in sheet resistance until the film is annealed at high temperatures mainly ranging from 300-600 °C the film does not turn transparent and decreases in sheet resistance without the annealing [6]. In such cases plastic or polymers cannot be the materials of choice for the substrate. According to the literature, polymers or plastics can be used as substrates in Ion Beam Assisted Deposition (IAD or IBAD). In which one or more ion sources can be installed with the deposition equipment to support the insufficiency of particular ions during deposition process [8]. In case of glass the varieties are widespread, the deposition process does not require to be implemented at room temperature, post deposition annealing temperature can be as high as 550 °C, higher temperature annealing values do not have any more significant results [9-10]. Stricter cleaning protocols can be implied e.g. use of strong acids and bases etc. this study shows very good results of post annealing of ITO deposited glass substrates, which will be discussed in detail in chapter 7.

3.2.2 Deposition Rate

The most important parameter to consider during ITO's deposition is its deposition rate. As mentioned earlier in Chapter 2 that certain materials undergo fragmentation in the process of evaporation by the electron beam, resulting in a different chemical composition from the initial material. ITO is one such material which disintegrates into different constituents during the deposition process, especially in case of the EB-PVD. Literature studies for such materials suggest a very low deposition rate [8]. The reason for which

is, that higher deposition rates involve higher beam current or power to bring the material into its molten state before evaporation. ITO is also a bit unique compared to conventional metallic materials, in the sense that it does not melt before evaporation for deposition, this helps understand that it is a volatile solid and needs little and very precise powers for evaporation [8-9]. Literature study suggested different deposition rates ranging from 0.05 nm/s to 0.25 nm/s, and related results to these depositions were also studied and applied. The best result claimed in the literature amongst the mentioned range was for the 0.05 nm/s. At this deposition rate it was learnt that the sheet resistance was least and the transparency was optimum [8-9]. Figures 3.4 and 3.5 helped to illustrate the dependence of resistivity and the optical transparency upon the deposition rate from the literature accordingly, which helped in deciding the best deposition rate for this application. The final thickness required for the film is dependent on the rate of deposition, in a way that thicker layers are hard to implement with very slow deposition rate. Not only more time is required but also vigilance and personal monitoring is needed during the deposition.

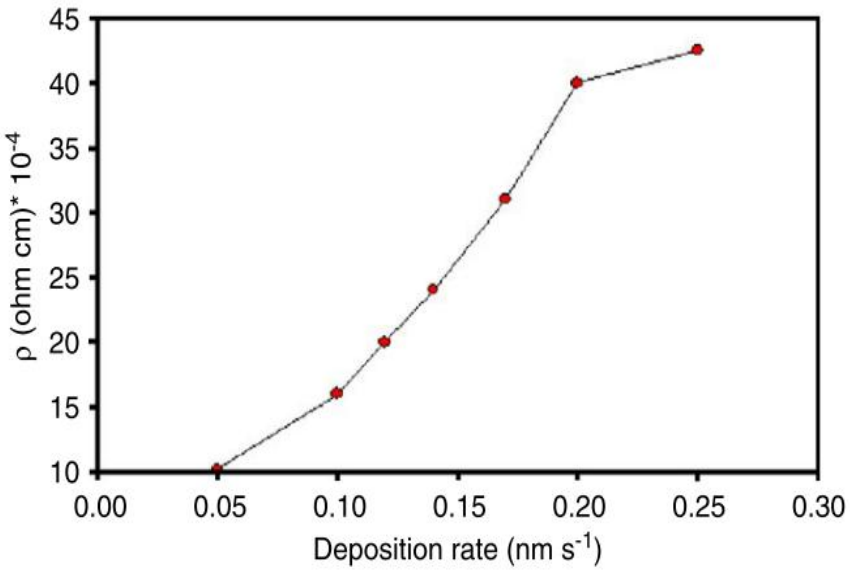

Figure 3.4: *The resistivity of ITO thin film as a function of the deposition rate [8].*

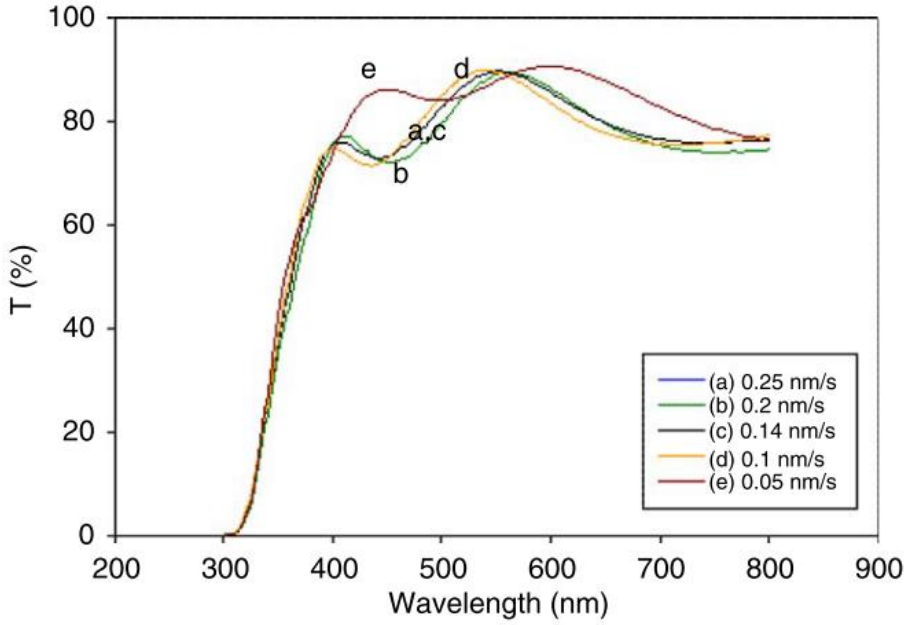

Figure 3.5: *The optical transparency of ITO thin film as a function of the deposition rate [8].*

3.2.3 Post Deposition

Thus the suitable deposition rate, once chosen helps to improve the odds of the film quality. During the coating process in the evaporation chamber if the heating and other ion sources are not used then for sure there needs to be post treatment of the film and substrate. The post treatment is done to optimize the film's structural and chemical insufficiencies. The most usual treatment is the heat treatment in presence of oxygen [8-9]. There are chemical treatments as well but they are to actually provide a better surface look for commercial purposes [10]. The post heat treatment of the film allows for it to achieve an optimized or decreased grain size and lattice constant, a better structural configuration in terms of phase composition, increase in the mobility and/or carrier density lower band gap energy and the films are crystalline having a (2 2 2) preferred orientation, in contradistinction to as-deposited films, which turn out to be amorphous. These improvements result in the films to be optically better transparent and electrically conductive or with lower sheet resistances. Figures 3.6, 3.7 and 3.8 can provide a better evidence of necessity of post annealing to deposition.

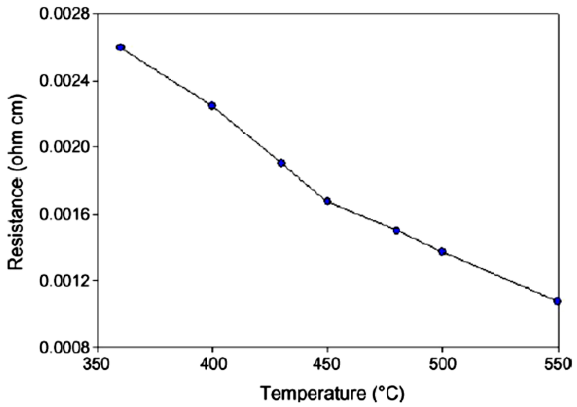

Figure 3.6: *Resistivity of films as a function of the annealing temperature [9].*

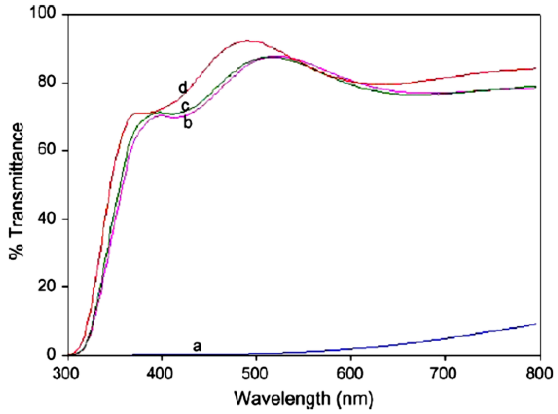

Figure 3.7: *The optical transmission spectra of ITO thin films (via 250 nm in thickness) at various annealing temperatures. (a) As-deposited, (b) 350 ℃, (c) 450 ℃, and (d) 550 ℃ [9].*

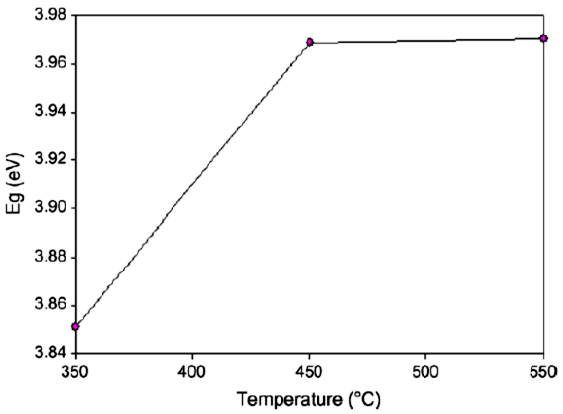

Figure 3.8: *Dependence of the direct allowed optical band-gap of ITO thin films on the annealing temperature [9].*

3.3 Biocompatibility of ITO

Since ITO has to be used to make MEAs, that will directly measure the electrical impulses from the cells it is of prime concern that the question of its biocompatibility is properly researched upon and understood. The literature study gave very promising evidence suggesting that ITO is highly biocompatible with quite extraordinary properties in terms of its cytotoxicity and protein adsorption capabilities.

Microelectrodes have the potential to become useful tools for recording from and or stimulating cells of the nervous system and heart for the purpose of medical innovations and studies. The electrodes are expected to remain functional for many weeks after a culture has been exposed over them; therefore, the material of the electrode must be compatible within their biological environment, so as to minimize complications and contaminations. In one of the studies, the biocompatibility of materials for electrode sites was investigated taking into account of two measures: a) cytotoxicity and b) protein adsorption. The cytotoxic effects of material on the cells were investigated using neutral red assay, and adsorption of proteins onto materials has been investigated using atomic force microscopy and ellipsometry [11].

The investigative study of materials for biocompatibility and bio inertness included gold (Au), platinum (Pt), iridium (Ir), ITO and titanium (Ti). Ti was chosen as a reference material since it is a long established implant material [9]. According to the literature after 72 hours of exposure to fibroblast cells, Au, ITO, and Ir showed no inhibitory effects on cell growth, whereas Pt and Ti showed greater amounts of growth inhibition. Likewise, protein adsorption to different materials showed a steady growth following the initial adsorption pattern, however 24 hours later of exposure to plasma, Ti had the thickest and ITO had the thinnest layer of adsorbed protein [11].

4. MICROELECTRODE ARRAYS

4.1 Introduction and Usage

The electrical activity of cells such as neurons and cardiomyocytes provide precise, detailed and fundamental insight, relating to their physiological and pathophysiological functions. Despite the well-known properties of these cells working in concerted fashion as tissues, organs and systems, details of single cell physiology and pathophysiology is still in its infancy. A lot of research is being done in order to seek a multi-channel approach, which could eventually bridge the gap for understanding the properties of single-cells alone, and in cellular networks. Thus the electrical activities of these cells need to be studied in both the modes, as single-cells and in networks (tissues). The study of the electrical activities can therefore be made, either through intracellular or by extracellular methods. The intracellular technique utilizes electrodes which are clamped or inserted inside the cell to measure the electric flux across the membrane. Extracellular measurement technique on the other hand makes use of external electrodes (mostly planar) that measure ionic concentration outside the cell membrane. Both the methods are capable of detecting simultaneous and inter-dependant activity of the cells, in response to environmental and/or contextual stimuli, which is crucial for cellular signalling. Consequently, when the need arises to simultaneously study the characteristics of cells in a network or as single-cells, at a high spatial resolution, microelectrode arrays will be required [12].

4.1.1 Definition and Applications

A microelectrode array (MEA) is a sensor, with an arrangement of probes (electrodes) in shape of plates or shanks, allowing passage of electrical signals from several sites in parallel of an electrogenic cell or a network, for either extracellular recording or stimulation. They serve more or less as interfaces that connect cells of body to electronic circuitry [12-14].

Excitable or electrogenic cells create ion currents upon excitation, causing a change in transmembrane potential. The electrodes present on a MEA transduce the change in voltage from the cell to electronic voltage which is measured by amplifiers and recorded (*in vitro* measurements). In general, MEAs are categorized in two categories: implantable MEAs, used *in vivo*, and non-implantable MEAs, used *in vitro*. Since this study addresses *in vitro* measurements *in vivo* MEAs or implantable MEAs will not be discussed. MEAs can be used to study almost all electrogenic cells and/or tissues for extracellular recording *in vitro*, for example, central or peripheral neurons, cardiac myocytes,

whole-heart preparations, or retina etc. [14]. The applications for MEAs in the fields of neurobiology and cardiac electrophysiology are numerous. Some of the main field neurobiological applications involve: Ion channel screening, drug testing, safety pharmacology studies, current source density analysis, paired-pulse facilitation (PPF), long term potentiation (LTP) and depression (LTD), input/output (I/O) relationship of evoked responses, circadian rhythm, neuro-regeneration, developmental biology, micro electroencephalograms (μEEG), and micro-electroretinograms (μERG). Similarly, some of the core main field applications in the cardiac electrophysiology involved are: Activation and excitation mapping, the measuring of the conduction velocity, the long term characterizations of cell types (especially stem cells), culture pacing, drug testing, safety pharmacology studies, monitoring of QT-related prolongation and arrhythmias, co-cultures and disease / implantation model etc. [14].

4.1.2 MEA Components and Usage

Initially, *in vitro* MEAs were fabricated using Au as the electrode material, which were platinized to reduce the high impedance and improve the signal to noise ratio. However, MEAs with such electrodes proved to be unstable over prolonged periods of usage, due to the surface Pt degradation, which eventually required to be re-platinized again in order to be used again. Standard MEAs today are fabricated with electrodes made up of Au, Ti Pt black and TiN (titanium nitride). TiN is the most famous and most desired amongst the rest for its good material properties and low cost. The insulation layers used can be either Si_3N_4 or SiO_2 of which Si_3N_4 is more common. The culture rings can be either plastic, glass or polydimethylsiloxane (PDMS), of which PDMS rings are preferred more as they are detachable and provide better cleaning after use [13].

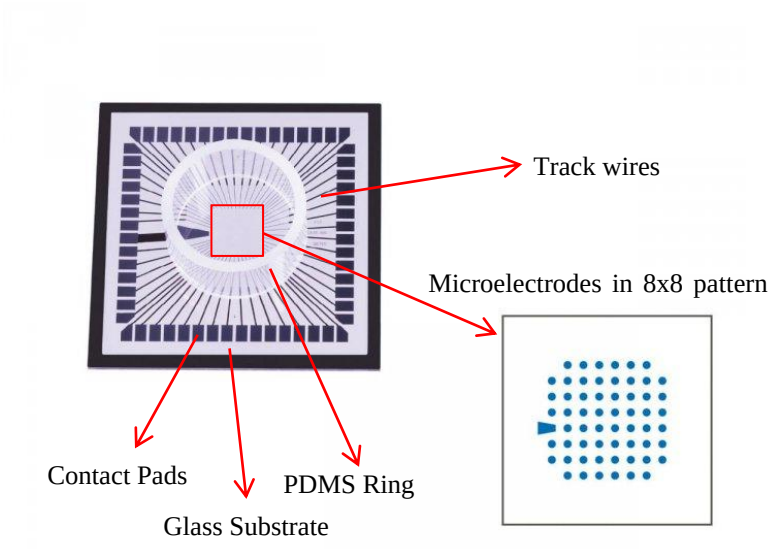

Figure 4.1: *Standard 8 x 8 MEA with a glass ring to hold the culture from Multi Channel Systems [14].*

A standard MEA generally consist of a transparent substrate, microelectrodes, track wires, contact pad, and insulation. The substrate material for a standard MEA from Multi Channel Systems (MCS) is generally glass or plastic with dimensions 49 x 49 x 1 mm (W x D x H) [15]. The standard MEA parameters explained in this section mostly refer from MCS, there can be different parameters for standard MEAs from other companies as well. Since MCS MEAs are used as standards for this study, thus MCS is discussed with special focus. The diameter of the standard microelectrodes can range from 10, 20, 30 μm, with the separations of 100, 200 or 500 μm [15]. The material with which, microelectrodes are generally made up of include TiN, ITO, Pt black, Pt, Au, Ti etc. [15]. However, MCS focusses only on TiN electrodes. The track wires connect the microelectrodes to the contact pads and are fabricated using ITO or Ti mostly [15] but other metals can also be considered. The contact pads provide an interface between the circuitry of the recording system and the microelectrodes. They are made of the same metal as the track wires but other metals can also be used. The insulation, which is used to isolate the track wires from each other and the buffer medium of the cell/tissue culture, is usually made of Si_3N_4 [14]. Figure 4.1 shows all the components of a standard 8 x 8 MEA very clearly, except the insulation layer as it envelops the MEA on the top surface leaving only the electrodes and the contact pads exposed.

Cultivation of cell lines or primary cell preparations can be done directly onto the MEA. Both acute recordings using freshly prepared slices or organotypic cultures can be cultivated on the MEA, however both require a culture medium which is usually provides buffering and nutrition for the culture. The culture medium solution also stabilizes the electrode tissue interface and stabilizes the impedance thereby lowering noise in the recorded signal. When the recording is begun, the signals are first amplified by a filter amplifier which is relayed to the data acquisition unit converting it to digital signals and then sent to the computer [14].

4.2 Types of MEA Layouts

There are several MEA layouts according to the number of electrodes and their arrangement. Different layouts facilitate different types of applications for recording. Increased demands for a specific biological need has increased development of more customized and unique layouts. A few of the conventional layouts are discussed in the subsections below.

4.2.1 Standard Line of MEAs

Standard MEAs available commercially, come in pattern of 8 × 8 or 6 × 10 electrodes with 60 electrodes. The characteristics of standard 8 x 8 MEAs are already mentioned quite elaborately in Section 4.1.2 and seen in Figure 4.1. However, 6 x 10 layout has not been focussed upon, it is sometimes referred to 6 Well 60 MEA as well. The 60 elec-

trode, 6 well MEA contains 6 wells that resemble distinct electrode chambers, with nine electrodes in each, positioned in a 3 × 3 grid. However, an internal reference electrode is present in each well making a total of 10 electrodes in each well altogether, therefore referred to as 6 x 10 as well as 6 well layouts. Figure 4.2 provides an illustration of what 6 well layout looks like. The diameter of the electrodes is 30 µm, and the inter-electrode separation distance is 200 µm for this arrangement.

Both the standard types of MEAs are used to study acute brain slices, single-cell cultures, and organotypic prepared cultures. An important fact about standard MEAs is that versions with an optional internal reference electrode along with different culture rings/chambers are available by manufacturers. This is assumed to accommodate separately individual needs either for acute recordings or long-term cultures, or even combining patch/intracellular approaches with MEA recordings. [13-14].

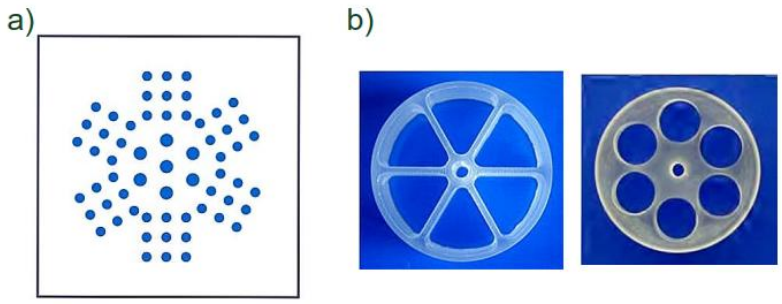

Figure 4.2: *a) Layout of electrodes in a 6 well or 6* x *10 MEA. b) Corresponding choices of PDMS rings to hold culture and culture media upon the electrode regions [15].*

4.2.2 Thin MEAs

When imaging needs to be combined, with MEA recordings, an introduction to “Thin”-MEAs become a necessary. Whenever, high-power objectives with high numerical apertures are in question, they usually end up having a very low working distance on the order of only some hundred micrometres. Thus the high-powered lenses of inverted microscopes are not able to image through the standard MEA due to the 1 mm thickness of the substrate. The solution to this problem can be addressed by fabricating MEAs that have been constructed using cover slip glass. Thus the name, “Thin”-MEA which has thickness of no more than 180 µm. Due to the fragile nature of the Thin-MEA it is mounted on a ceramic support to prevent breakage, while being used with high-powered objectives. The conductive leads and contact outer pads of a Thin-MEA are manufactured using ITO, Figure 4.3 shows a picture of Thin-MEA [13-15].

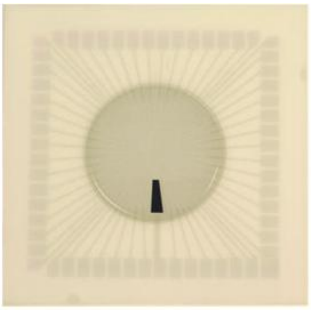

Figure 4.3: *A picture of a Thin-MEA from Multi Channel Systems with transparent ITO tracks and contact pads [15].*

4.2.3 2 x 30 MEAs

The requirement to study the local responses of two specimens of cells or tissue cultures side by side, at high spatial resolution gives way to 2 x 30 MEA layouts. There are 60 electrodes of 10 µm diameter in this layout and are arranged into 2 groups of 6 x 5 electrode pattern. The two groups of electrodes are 500 µm apart from each other, and 30 µm of inter-electrode spacing is present within each group. This arrangement of electrodes allows an unparalleled insight into local connectivity and interconnectivity over a wide range of 500 µm. Thus these MEAs are being used to record multi-unit activity, of a retinal neuron as a two-dimensional multitrode sensor, giving rise to improved spike separation. More than one electrode of the MEA can pick up the activity of this single neuron due to the small inter-electrode distances. Since electrodes vary slightly in distance for the same neuron, each electrode records a slightly different waveform from at the same time point. Thus a better and more precise study of a single cell is possible in a multi-dimensional fingerprint-like pattern, rather than one-dimensional waveform based conventional spike sorting analysis [13-15].

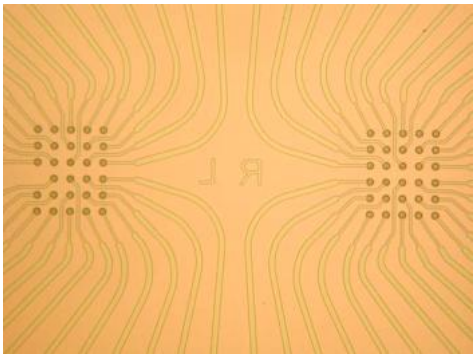

Figure 4.4: *A layout of 2 x 30 MEA with flat round electrodes made of TiN, tracks and contact pads made of transparent ITO and insulation material is Si_3N_4 from Multi Channel Systems [15].*

4.2.4 High Density MEA

When spatial resolution is of utmost importance, and conduction velocity or synaptic delays are to be studied precisely over prolonged distances “High Density” (HD)-MEA are used. They compose of the high density of electrodes for instance up to 256, with the diameters of 30 or 10 µm covering a large area of 2.8 x 2.8 mm^2, with inter-electrode separations of 30, 60, 100 or 200 µm. Thus, providing the necessary high enough spatial resolution over large distances. They are used mainly for unique studies such as the delayed synaptic response in ganglia. Figure 4.5 shows the picture of an HD MEA with its 16 x 16 layout of electrodes [13-15].

There are other layouts available as well, both commercially and under scientific development by research scientists for unique applications. However, the most common ones which were related to the thesis study are discussed here.

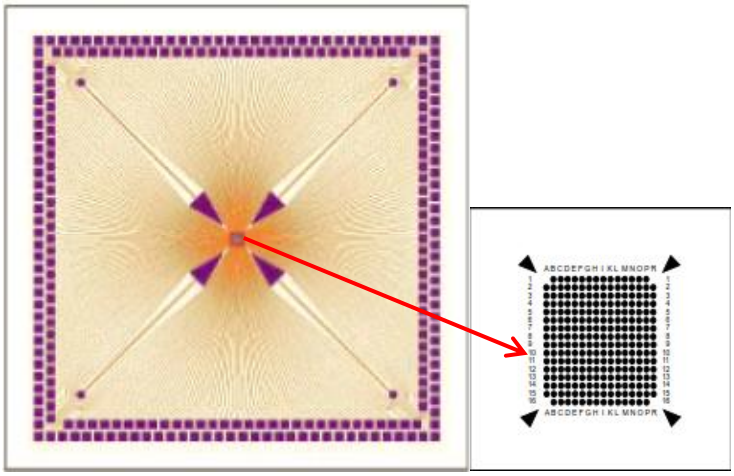

Figure 4.5: *Picture of an HD-MEA with 256 electrodes made of TiN, wires and contact pads made of ITO and insulation of Si_3N_4 from Multi Channel Systems [15].*

4.3 MEA Fabrication and Evaluation Concepts

4.3.1 Fabrication Conceptualization

Ideally speaking, microfabrication techniques employed should be such as to allow production of MEA biochips with significant cost reduction due to smaller MEA chip dimensions. However, this is just impossible at present, due to insufficient technological advancement to turn MEA biochips into single-use disposables. Nevertheless, there are still technological improvements underway that can be done in order to achieve this goal in the near future. Till that time, compromises need to be made in order to produce high quality MEAs which if not disposable, are at least reusable for a sound number of times. Conventional techniques for microfabrications commercially at least, have

stretched to the border of compromise ensuring production of high quality MEA by the least possible cost using automation and bulk productions.

For research and development, the in house fabrication of MEAs in the research facilities of academic institutions, the costs are higher as here the man hours utilized for production of limited quantity owes the most cost. Though the processes in the commercial production and research facilities are more or less the same, the large scale production in parallel and automation brings all the difference.

4.3.2 Fabrication Techniques and Material Evaluation

For manufacturing MEAs in general the techniques needed are more or less the same in most cases. The possible techniques used for manufacturing typical MEAs are

1. Metal or Electrode Material Deposition
2. Photolithography
3. Etching Processes: Wet, Dry and/or Liftoff
4. Cleaning Protocols

These are the major categories of technologies used, sometimes not all are necessary and at other time all are employed in different combinations and iterations.

The most essential concern for evaluating MEAs during manufacturing and after it is, to consider all the component materials that will be used in the fabrication and their respective evaluations individually along with final evaluation as MEA. The materials to be considered in MEA fabrication involve materials of;

1. Substrate
2. Electrodes
3. Track wires or Leads
4. Contact pads
5. Insulation
6. Culture Chamber or Containment Rings

All these parts must be thought through before beginning the fabrication process. The consideration for these materials depends on the application for which the MEA will be used, for quality and longevity of use and the biocompatibility. It is therefore absolutely necessary to evaluate MEA on the basis of material properties and characteristics.

The biocompatibility is extremely important for all the materials that will be in contact with the cell culture or tissue, to show no toxic effects, nor affect the cell’s “well-being” during the entire experimentation. Furthermore, the materials should allow a good adhesion of the biological preparations. Biocompatibility should be examined experimental-

ly for unknown substances, however today almost all materials that are related to MEAs have been studied [13-15].

Good electrode characteristics of the electrodes should allow the measurements of small signal amplitudes with a good signal-to-noise ratio. Therefore, the impedance testing and noise measurement of electrodes after manufacturing is extremely important. The lower the impedance, the lower the basal noise for voltage measurements. The sheet resistance of the electrode material should also be measured after a deposition process [13-15].

The MEA biochip should be as transparent as possible in order to enhance observation using an inverted microscope. Furthermore, if the electrodes are made from transparent material, optical (potentiometric dyes) and electrical measurement can be combined in one single experiment. Otherwise plain transmittance measurements using spectrometer can be done for analysis [13-15].

Material testing of MEAs includes: studying the hysteresis of electrodes due to temperature changes and PH changes of buffer. The topological studies of electrodes using Scanning Electron Microscope (SEM), Atomic Force Microscope (AFM) measurements of surface roughness, X-ray diffraction crystallography to ensure the material crystal orientations are as they are supposed to be etc. [13-15].

5. PHOTOLITHOGRAPHY AND ETCHING PROCESS

5.1 Basics

Photolithography is one of the key the processes used in microfabrication to pattern precise geometric parts of a thin film or the bulk of a substrate; it is also referred to as optical lithography or UV lithography from time to time. The basic principle of photolithography utilizes light to transfer a geometric pattern from a photomask to a light-sensitive chemical called photoresist (sometimes also referred to as resist), on a substrate of interest. Using different chemical or physical processes can then engrave the exposure pattern into the substrate or the bulk material, or in other cases facilitate deposition of a new material in the desired pattern upon the thin film/bulk material underneath the photo resist. The process is repeatable to form as many patterns needed over as many successive layers of thin films. As an example, modern integrated circuitry could utilize the process up to 50 cycles or more, just for the microfabrication of a simple CMOS chip [16].

Like photography, photolithography depends on the same fundamental principle where the pattern in the etching resist is created by exposing it to light. The exposure can be done either directly, without using a mask or with an image projected using an optical mask. It can also be compared to a more specific and precision version of the method used to make printed circuit boards, where the subsequent stages of the process have more to do with etching than with lithographic printing. The hallmark of the process is that it can create extremely small patterns, which can have geometric dimensions as small as tens of nanometres in size. It not only facilitates a very precise resolution in geometry but also affords exact control over the shape and size of the objects needed to be created. This process is also accredited for creating patterns over an entire surface cost-effectively. Though it stands out in many other areas like precision and small dimensions, photolithography has a lacking that it requires a flat substrate to start with; it lacks effectiveness when it comes to creating shapes that are not flat, and often requires extremely clean operating conditions [16].

Photolithography process is most extensively used for transferring geometric shapes on a mask to the surface of a silicon wafer, but it can also utilize other substrates commercially and academically. The steps involved in the photolithographic process include wafer cleaning, barrier layer formation (specifically for silicon substrate), photoresist application, soft baking, mask alignment, exposure and development, and hard-baking

[16]. Thus a single iteration of photolithography can combine all the mentioned steps or some of them in sequence. Modern cleanrooms can be fully automated or semi-automated, utilizing robotic wafer track systems to coordinate the process. The procedure mentioned, however do not review other advanced treatments, such as thinning agents or edge-bead removal etc. [16]

5.2 Cleaning

Usually organic or inorganic or both contaminations are almost always present on the wafer's surface, and needed to be removed by wet chemical treatment, RCA clean procedure is a good example of chemical treatment as it utilizes solutions containing hydrogen peroxide. Other cleaning protocols and solutions can also be used that include trichloroethylene, acetone, methanol or ethanol. Cleaning protocols can vary according to the substrate type, however protocols are usually generic and can be the same for similar type of materials e.g. all glass substrate can use the same cleaning protocol [17].

5.3 Preparation

The preparation of the wafer requires some initial heating to a temperature sufficient to eliminate any moisture that could result after the cleaning procedure or storage, a temperature of 150 °C for ten minutes is sufficient for that matter. Stored wafers for prolonged periods of times absolutely require cleaning procedures before preparation to apply photoresist. Adhesion promoters either liquid or gaseous can be applied such as, Bis(trimethylsilyl)amine hexamethyldisilazane, (HMDS). When applied to the surface it promotes adhesion of the photoresist to the wafer. The Silicon dioxide surface layer of a silicon wafer reacts with HMDS to form a highly water repellent layer by forming a compound tri-methylated silicon-dioxide on the surface. This water repellent layer helps during the developing stage, when it prevents the penetration of the aqueous developer between the photoresist layer and the wafer's surface, thereby preventing the so-called lifting of small photoresist structures present in the (developing) pattern. Ensuring a better development of the image requires that, the promoter layer is best covered by the surface of the wafer and then placed over a hot plate to dry while at a stabilizing temperature of around 120 °C approximately. The application of a promoter layer such as HMDS isn't always necessary, for instance for developing over glass slides using good quality photoresist might not require us to go through this step at all. Instead it has to be ensured that the glass is absolutely clean and if possible to be treated by oxygen plasma to provide decontamination for organic contaminants as we all making the glass surface hydrophobic, which more or less also gets the job done just as well [17]. In the research work for this study the latter was done over using the HMDS.

5.4 Photoresist application

Once the cleaning and preparation of the wafer is done the next step is to cover the surface with photoresist, which is done by spin coating. Photoresist is generally very viscous; the solution of photoresist is therefore dispensed over the wafer and then spun at high speed ensuring a uniformly thick layer over the entire surface of the wafer. The spin coating typically utilizes speeds between 1000 to 6000 rpm for a duration of 30 to 60 seconds, which in turn is able to form a layer that can vary from less than 100 nm to tens of micrometres in thickness. Once the resist is applied after spin coating the resist coated wafer is subjected to a session of prebaking to drive off any excess photoresist solvent, usually the temperature is set between 80 to 150 °C for a short interval ranging from 1 to 3.5 minutes on a hotplate or tens of minutes in oven depending upon the resists instruction for usage. [17]

5.5 Photoresists, Exposure and Developing

After the application of photoresist and prebaking, the resist is exposed to intense light almost always following a very precise pattern. This exposure due to light causes a chemical change in the photo resist that allows part of the photoresist to be removed when placed in a special solution, called developer, just as in the case of a photographic developer. The light for exposure is usually exposed as a pattern which uses the photomask or the sometimes also referred as mask. Photomasks are usually opaque plates having holes or transparencies that give passage to through the light in a defined pattern. As for the photoresists, they comprise of two types; a positive resist and a negative resist both have opposite reactions upon exposure to the light. A positive photoresist becomes soluble in the developer when exposed, there by leaving an impression of the unexposed resist after developing. Contrarily, a negative photoresist remains undissolved upon exposure; in fact the unexposed regions are soluble in the developer, thus leaving the impression of the exposed part. [17]

5.6 Photomasks

A photomask (or simply mask), is a plate with optical transparencies that allows light to shine through in a defined pattern, in order to provide projection over a photoresist. Masks in photolithography are used to provide pattern over the photoresist that needs to be patterned by etching, following the developing process. The pattern on the mask varies for the types of resist used, for a positive mask the geometry projected will be totally opposite in comparison to a negative resist. Therefore, the pattern of the mask is governed according to the type of resist used. The pattern for the mask is designed from a computer program a data file. This is then converted into series of polygons and written either, onto a square of fused quartz substrate covered with chromium or over PET (Polyethylene terephthalate) film as base material. For chrome masks the fused quartz

substrate is covered with a chromium layer using photolithographic process. A beam of laser or electrons is used to expose the pattern defined by the data file and travels over the surface of the substrate. The photoresist on the mask at the area of the pattern is exposed, the chrome is then etched away, leaving a clear path for the illumination light in the exposure and alignment system to travel through.

The film masks utilize the PET film and the computerized data file with the pattern is simply printed with a high definition laser jet printer with opaque ink. The printed part on the mask is opaque and attenuates the exposure through illumination light of the exposure and alignment system [17-18].

5.7 Etching

Etching is the process, where the chemical agents help in removing the uppermost layer of a particular substrate, precisely from the regions that are unprotected by a photoresist. There are two types of etching processes used in the lithographic process, wet etching and dry etching. In wet etching liquids are used to etch the upper and unprotected surfaces of the substrate, whereas, a gas of ions (usually plasma and reactive gases) is used in dry etching to achieve a similar effect. Wet etching processes generally result in isotropic etching of the surface, which is often vitally important for microelectromechanical systems, where suspended structures are required to be patterned from the underlying layer. However, dry etching techniques are generally an isotropic in nature, and are use so, to avoid significant undercutting of the photoresist pattern. It is especially utilized when the width of the geometric features needed are defined as similar to or less in magnitude than the thickness of the substrate layer being etched [17].

Furthermore, ever-smaller and precise geometric features defined photolithographically using the resist are transferrable to the substrate material. These geometric features are being patterned in the semiconductor technology by the development of low-defectivity anisotropic dry-etch process [17].

5.8 Photoresist removal

Once the etching process is done, the photoresist is no longer needed and must be removed or stripped from the substrate. This usually requires a liquid resist stripper, which chemically changes the resist so as to, that it no longer adheres to the substrate. Photoresist can also be removed by a plasma containing oxygen, which actually oxidizes the resist. This is called the ashing process, and resembles dry etching. Some resist strippers dissolve the hardened resists, e.g. use of 1-Methyl-2-pyrrolidone (NMP) solvent is one such example. Acetone is also known to be a universal solvent and is many a times used to dissolve positive and negative photoresists alike. It is also cheaper than many other resist strippers to use and often preferred as an economical alternative [17].

6. TIER I: ITO FILM DEPOSITION

Once the theoretical knowledge was reviewed and acquired for the thesis, the practical part was planned in a 3 tier plan, the 1st tier included the formation of transparent ITO thin layer on glass substrate, the 2nd tier of the thesis involved in the patterning of the same transparent thin ITO layer into microstructures needed in MEAs and the 3rd tier involved the optimizations of step for final Standard 8 x 8 ITO MEA fabrication. In the first tier of the thesis the experimentation involved in the processes of coating thin layers of the ITO over microscope glass slides using different deposition rates from the EB-PVD device at our disposal in the lab, baking (annealing) the coated slide at high temperatures ranging from 300 to 550 °C and studying the transparencies and the sheet resistance of the ITO layer. In the second tier, experimentations related to techniques for patterning the films of ITO on glass substrate were studied. The aim was to fabricate microstructure small enough, which are present on MEAs is described, and that involved in wet and dry etching experiments of ITO. This took the longest time in the thesis study other than the writing part of course. In the third and the last tier successful mixes of the first and the second tiers were used and microfabrication of MEAs with optimization of microfabrication processes according to ITO manipulation was done. Finally, in the end, a design of eight prototypes of standard 8 x 8 30/200 (30 μm diameter and 200 μm spacing) MEAs was possible.

6.1 EB-PVD and Metallization Device Usage

The practical plan in the beginning was supposed to involve deposition of ITO using an ion source with the EB-PVD device present in our lab which we also refer to as the “metallization device”, but due to the unavailability of the ion source it had to be revised, the methodology, in a way so that the deposition wouldn’t require the use of the ion source. Instead a strong literature evidence suggested that the ITO’s two main qualities of interest from the perspective of making MEAs mainly, the transparency and the sheet resistance were affected by deposition rate of the metallization device and the post heat treatment or annealing of the glass substrate and the ITO film [80]. In the literature it was stated that the best result for the deposition rate was observed at 0.05 nm/s and similarly the best result in terms of annealing was observed at 550 °C. The very first experimentation carried out for that matter was intended to utilize these two starting parameters as guides. The researchers of the literature used a furnace for annealing their samples but due to the unavailability of a furnace in our lab a hot plate that operated at 400 °C initially was used, which resulted in the first good result. However in later experiments the annealing was carried out using a furnace with temperatures up to 550 °C.

Further explanation is provided in the following subsections of this chapter. In order to begin the work for Tier I, a thorough training to use the EB-PVD device was acquired from Mr. Tomi Ryynänen who demonstrated both, the use of the device and also troubleshooting general problems. Ability of using the metallization device is one the core steps in the processing of microfabrication of this study.

Metallization device can be used to deposit quite a few materials such as metals and certain compounds including ITO into thin films as explained in the previous chapter related to EB-PVD of the thesis. However, in the case of ITO it needs special attention and constant diligence since ITO needs very slow deposition rate and normally it takes from 4 to7 hours of deposition depending upon the thickness of the film.

6.1.1 The Literature Study for ITO Deposition

The experimental study initiated with the Tier 1 that is ITO deposition and ensuring that the film becomes transparent. Previously some work was done in this regard but the results were not all that successful. So the very first challenge at hand for this study was to make our ITO transparent. The literature search that was made mostly involved use of ion sources for transparent deposition of ITO or heated substrate deposition to obtain transparent ITO films on substrates. Fortunately, then two articles from the same authors on ITO deposition using EB-PVD and post heat treatment were referred to and immediately experimented practically [8-9]. ITO deposition isn't usually done using EB-PVD in fact magnetron sputtering and RF sputtering are usually the choices of deposition for ITO [14]. The information in the two articles discussed mainly of the structural, electrical and optical properties of indium tin oxide thin films annealed for 1 h at the temperature range from 350 to 550 °C in air and at low deposition rate of 0.05 nm/s. Their results showed relatively high electrical conductivity such as $7x10^{-4}$ Ω cm and high visible transmittance (above 93 %) obtained using electron beam evaporation technique, just as was needed in this study. Their XRD results also included in the literature mentioned that the crystallinity of ITO thin films was improved with annealing thin films with 37 nm in diameter grain size obtained at 550 °C, which was a much needed thing since the ITO granule used to deposit ITO films in our metallization device are amorphous and for MEAs the electrodes and the tracks should be crystalline for long term and robust use as in crystalline form ITO is reported to have better characteristics [8-9,19]. Particularly, both the grain size and the optical band gap decreased with increasing deposition rate, while the lattice constant increased [8-10]. The results showed that by decreasing the deposition rate, the conductance of the ITO thin films was increased [8]. The DC conductivity in the ITO thin films is also well observed in the 350–550 °C range as well. Their results also showed that by increasing annealing temperature, the conductance in ITO thin films was increased, which is again another plus point when we need to design electrodes. Further, from their results it was concluded that the deposition rate and annealing temperature plays a major role in controlling the electrical

properties and the optical transmittance of the ITO films with the right mix of both [8-9]. Their extensive study also included a comparison between the EB-PVD and other deposition techniques, which showed that the better figure of merit value could be obtained by EB-PVD. Thus referring to these two articles gave a clear direction in how to proceed with the work and progress further. Most of the time and efforts in the Tier 1 were utilized in validating the results from the article and evaluating if they were valid or not. Thus the main components of Tier 1 involved utilizing metallization device for ITO deposition, developing cleaning protocols for glass substrate, annealing and heat treatment of post deposited ITO thin film on glass substrate, and measurements of transparencies and sheet resistances of the ITO films deposited over glass substrate.

6.1.2 The Pilot Run

The very first time the deposition of the ITO thin film over glass was carried out, the guidelines of the literature were followed to the closest possible extent which included deposition with 0.05 nm/s as it showed strong promise for success [8-9]. The deposition process included training on the metallization device and a pilot run for the deposition of ITO. The process took almost an hour, since the thickness for the pilot run was decided to be 100 nm. Based on 0.05 nm/s deposition rate, 100 nm thick layer required 33.33 minutes in total deposition time theoretically. However, the device needs time to pump vacuum in the beginning of the run and pump clean N_2 gas at the end of the run which takes almost 30 to 40 min additional time of the process. Another very important and time consuming step includes of the mounting substrates over the substrate holder which in our device is in shape of a disc shown in figure 6.1 also takes about 15 to 25 minutes depending upon the number sample to be loaded onto the substrate holder. Thus for that first procedure it took some time over an hour approximately.

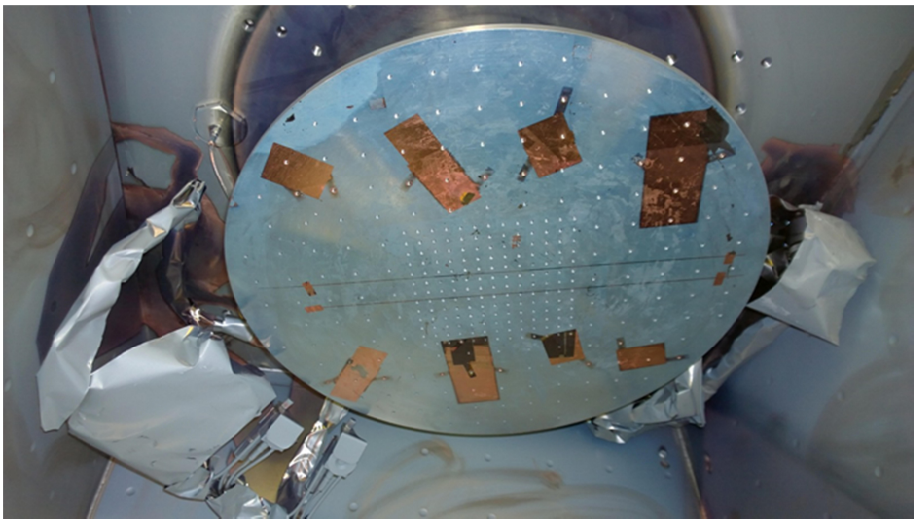

Figure 6.1: *Substrate holder of the Metallization device in the Clean room*

6.1.3 Operating the Metallization Device

The EB-PVD device in our Lab, shown in Figure 6.2 has a large chamber where the EB-PVD process takes place, within the same chamber there is a crucible control unit that has a capability to hold six crucible liners with the material required for deposition. The crucible control unit is rotatable only in one direction that is clockwise by the help of a controller panel in the operational rack of the device. The crucible rotor rotates via motor and chain driven system. The crucible rotation rotates at various speeds as well and can be operated automatically by automatic control that is assigned for a material to be used every now and then. The control rack of the EB-PVD device has a CPU and an LCD with Windows XP and touch screen LCD and a peripheral keyboard and mouse. Apart from that it has connections to all the sensors in the device. The control rack apart from the CPU, touch screen and keyboard has multiple controlling panels amongst which is the panel for crucible control and rotation, another panel for high voltage transformer and controller that powers the transformer to generate 12 kV of potential difference for operation. A TT controller for setting the beam current and anode voltage during the deposition that affects the deposition rate. Apart from that there are two more panels but for our understanding and operation these panels suffice our job for getting the deposition done.

Figure 6.2: *EB-PVD Device also known as Metallization device.*

The deposition can either be done manually or by automatic programming for a particular material. Same is the case of pumping vacuum and nitrogen before and after every deposition run. I personally have used both and prefer the automatic pumping as well as automatic deposition program. The reason to prefer automatic pumping in my case is that it involve less human intervention so less human error or chance to fumble. In case

of using an automatic programing for deposition that too helps in getting a more stable film with a uniform and smoother surface. In the manual mode the beam current needs to be adjusted every now and then to maintain a stable deposition rate. Whereas it remains controlled by a crystal feedback system in the automatic program thus giving us the freedom to observe and maintain the beam shape and orientation during deposition.

6.1.4 Setting-up Automatic Programing for Deposition

In the automatic programing, the program is set for a different material or film with information of the material like the density of material, rate of deposition, maximum power of beam, minimum power of beam, z ratio of the material, pocket of the crucible with the material, etc. All these variables are to be punched in before using the automatic program. It is of extreme importance that the person who is setting up the program is well-versed to the material properties of the material for which the program is being set. It is also advisable that the user also knows the safety limits of the device's working range to avoid damaging the samples as well as the metallization device. With all the necessary material and device details punched in, to make an automatic program, the program is finally ready to be used.

6.1.5 Considerations of Beam Focusing

As the automatic program is being run the operator must be vigilant that the beam is focused onto the crucible and that it covers the whole crucible. Otherwise a beam concentration on a very small area of the crucible can cause the beam power to penetrate all the way to the end of crucible. This may cause to eat the graphite of the crucible or any metal if the crucible is metallic rather than a graphite one. A severe contamination of graphite onto the film is thus very much possible. To avoid this during the experimentations for ITO depositions, it was necessary to re-orient the beam placement and concentration after every 50 μm thickness increased for the ITO film on the substrate. It helped to make sure that the deposited film was never getting contaminated, and with that, the deposition rate also doesn't falter after the ITO granules kept on evaporating from the crucible uniformly. It is worth understanding that, a material like ITO that directly sublimates or evaporates without melting, the power of the beam for it, needs to lower gradually with the process. However, if a stable deposition rate was to be maintained, it was better to keep on shifting slightly the focus of the beam on crucible in a way that the evaporation of the ITO granules in the crucible remained uniform rather than in the middle alone. The ITO granules in the middle of the crucible evaporate much faster, if the beam is not shifted regularly around the crucible span. This was one of the most crucial points of the training, as this problem seldom occurs when metals are deposited.

6.1.6 Considerations for Substrate Loading

Another important consideration when using the metallization device for ITO deposition was that the glass substrates were always loaded on the circumference of the substrate holder. The reason for that was learnt when loading the substrate on the substrate holder for the first run, Tomi Ryynänen (the supervisor) suggested not only to load the test microscope slides in the middle of the substrate holder (plate), but also to load some substrates on the circumference of the substrate holder. At the time that seemed pointless owing to no prior experience in deposition. It was just a means of precautionary observation to notice any difference due variance in radial distance on the plate. When the deposition run was complete the ITO coated on the glass slides appeared shiny black and completely opaque. There seemed no difference between slides mounted in the middle of the plate compared to the ones loaded on the circumference. For reference purpose it is also important to mention here that just plain deposited ITO film on glass substrate or any other substrate for that fact, using EB-PVD is also termed as as-deposited and the figure 6.3 shows the result of our first as-deposited 100 nm film of ITO on glass slides. It should be also understood that as-deposited ITO film is before heat treatment and that there was no heating also during the deposition, neither was any ion source or ion exposure was present [8-10]. From here onwards as-deposited film must be understood as simple and pure deposition of ITO with the metallization device. These as-deposited samples were then annealed for an hour at 400 °C at which point they were no more as-deposited sample but annealed transparent ITO films over glass slides. At that time, it was observed that some slides were completely transparent compared to others which had some black cloudy blotches over their surfaces. The initial observation led to the hypothesis that the cleaning procedure might not have been as impeccable as it should have been. After a couple of more deposition it was conceived that the cleaning protocol wasn’t the only reason of the sample with the black cloudy blotches instead it was the samples in the middle that had the most blotches then the ones between the middle and the circumference of the substrate holder. However, the samples on the very circumference of the substrate holder were all completely transparent. Here the wisdom of loading a few sample on the circumference and adhering to an experienced advice paid off. After that it was always done so that the samples were loaded only on the circumference of the substrate holder.

It was also a mystery why there were blotches on the samples mounted in the middle of the plate compared to the samples mounted on the circumference of the plate. The literature review gave an elaborate overview that the structural orientation of the ITO film needs to be (222) at the lattice level and their observation of XRD (X-Ray Diffraction) analysis showed peaks at (222) for the crystalline ITO after annealing. Glance angle deposition is another form of EB-PVD where the substrate is held at an angle to assist in rough and porous films [20-22]. Thus this explained mystery of mounting the substrate on the circumference of the plate instead of mounting it on the middle.

Figure 6.3: *Samples of clean glass slides with as-deposited ITO by EB-PVD device.*

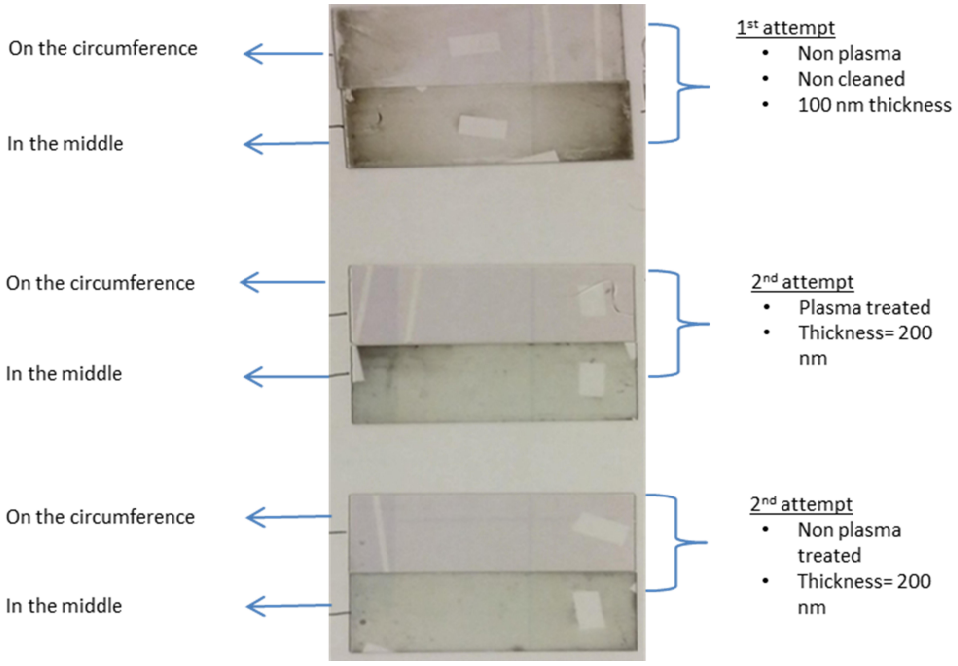

Figure 6.4: ***(Top)*** *Results of uncleansed slides pilot run,* ***(middle)*** *Protocol cleansed glass slides with post deposition plasma,* ***(bottom)*** *Protocol cleansed glass slides without post deposition plasma.*

6.2 Cleaning Protocols for Glass Substrate

Cleaning the substrate before deposition is of key importance. If the substrate is not cleaned thoroughly and properly it causes the material filmed on the substrate to break off the substrate. An unclean or non-ideally cleaned surface does not provide the film atoms the adhesion required to stick with the surface atoms of the substrate. For that very reason the fixing of the film on the surface is not optimum thereby causing unreliability of the film and its characteristics that might be required. If a referral back to figure 6.4 is made, it would be obvious that in the very first attempt the substrates were only wiped with isopropanol (IPA) which is neither a very standard operation of clean-

ing nor is it a thorough one. As a result, the slide that was mounted on the circumference did not also have the best result as in the case of 2 attempts. From this it was understood that the cleaning of the substrate was of prime importance and needs to be taken care off in the best possible manner. Thus came our glass cleaning protocol from a mixture of protocols.

The cleaning protocol was refined compared to just wiping the glass wafer with IPA soaked napkins. The new cleaning protocol still included IPA since it was abundantly available in our lab rather than ethanol which is another alternative, and an inclusion of acetone was made prior to IPA and as last part of keeping the clean slide under oxygen plasma for 5 minutes as the final step was decided. The oxygen plasma was produced in reactive ion etching device present in our lab. The oxygen plasma not only cleans any unseen organic or inorganic material of the glass surface but also helps activate the surface of the glass slides and made them more adhesive to the ITO atoms during the evaporation. Thus the refined cleaning protocol was finalized as follows;

1. First the glass slides were immersed in acetone reservoir of the ultrasonic bath for 5 minutes.
2. Then they were ultrasonically cleaned in IPA for 5 minutes.
3. Next they were rinsed with distilled water.
4. Then they were dried off using clean nitrogen blasts
5. Finally the dried glass slides were subjected to oxygen plasma for 5 minutes.

The same protocol will be used not only before the ITO coating of the glass slides but also in many cleaning steps in the microfabrication of MEAs. However, the final step of oxygen plasma will not be used in photolithographic processes and other time when cleaning is required for the glass wafers or MEAs. The final cleaning step of our microfabrication will again utilize the oxygen plasma as after that the MEAs will be formed and ready to be handed to the heart group to measure and analyse them.

6.3 Annealing & Heat treatment of As-deposited Films

Once the usage of the metallization device and the cleaning protocols were perfected the next logical step was to test the annealing temperature effects on ITO thin film which were needed to study and experimented with. By this time, it was conclusive that this deposition rate of 0.05 nm/s will remain fixed for all my depositions as it already showed the desired results in the first couple of pilot runs. It was only logical to keep the thickness of the film also constant for all deposition here onwards till further study could deduce which temperature yielded the best results for theses experimentations.

To study the annealing effects on the as-deposited ITO thin film the initial plan according to the availability was to use a hot plate in the lab that could reach temperatures as high as 450 °C. Even though according the literature search 550 °C should yield the

highest transparency as well as the least sheet resistance, but due to unavailability of a device to yield that high temperature it was decided to limit the study plan to 300-450 °C span. Later on a furnace with temperatures higher than 800 °C was made available, and the range was studied for entire 550 °C range.

Two initial experiments were conducted to start the study of annealing of ITO as-deposited 350 nm thin films. In the first experiment, a 100 nm ITO as-deposited glass slide was placed on a hotplate at 400 °C for an hour, since 400 °C had a successful history in [8]. However, the very first experiment also included glass slides that were not cleaned properly using the cleaning protocol so thoroughly explained in the last subsection. The result of the first annealing experiment is shown in figure 6.4 and better in figure 6.5 below.

The purpose of this first experiment was to actually find out if both our deposition and annealing worked even to the slightest extent. Previously ITO has been also experimented with in our research group but had not yielded much luck after annealing at 300-350 °C. Luckily the first experiment showed very promising results especially in the case of the slide that was mounted on the circumference of the substrate holder.

Figure 6.5: *Pilot run experiment for deposition rate and annealing for uncleansed slide.*

With this result it was safe to assume that the literature source was valid for both deposition rate as well as the annealing to some extent. Even though the result wasn't very good, for which there were more than a few reasons, amongst which the quality of the hot plate and the cleanliness of the glass substrate was one of the prime reasons. The surface of this particular hot plate was in reality not very smooth and even thus the heat distribution also varied, at some close observation it was seen that the glass slide wasn't even in contact with the surface from certain places. This only made more sense after the hour of annealing ended and the result of annealing was observed in the Figure 6.5. To get a better understanding of the right hand side black blotches on the slide mounted on the circumference of the plate was the part where the slide wasn't in proper contact with the hot plate during annealing. Thus the non-uniformity in transparency since that side did not have the same temperature as in the middle of the slide that was in better contact of the hot plate, refer to the Figure 6.6 below.

Figure 6.6: *Non uniform blotches in the annealed ITO film on the right hand side.*

In the second experiment, the glass slides were pre-treated and cleaned according to the cleaning protocol mentioned in subsection 6.2. The ITO deposition was done at a rate of 0.05 nm/s and the thickness was maintained at 200 nm. For annealing this time another hotplate was used, a better one, both in terms of surface quality and with slightly higher temperature span. The annealing temperature however was set for 400 °C, to observe better results. The thickness was set twice as much from the last time, the reason for that was, for the first experiments it wasn't clear if increasing the thickness would decrease in the transparency by increasing the black semi-transparent blotches that were observed in the pilot run. Another small deviation was also tried in the second experiment, before annealing a sample of as-deposited slides from the middle and the circumference of the plate were exposed to oxygen plasma up to 5 minutes. This small additional process was done to see if there was any effect of the oxygen plasma prior to annealing. In case of ITO, for improving the transparency of the samples, it is beneficial to expose the films to oxygen ions or allow deposition in the presence of oxygen at certain pressures [8-9].

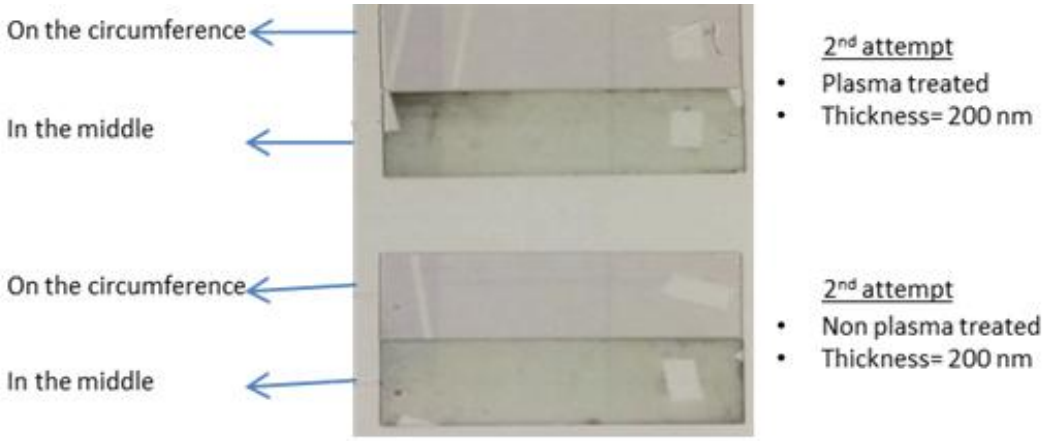

Figure 6.7: *Second run with cleaning protocol, deposition rate and annealing at 400 °C.*

Apparently oxygen plasma treatment didn't really have any significant effect on the transparency on the first look after annealing. However, the annealing temperature of 400 °C and the one hour time gave a very good apparent result, which has been seen in Figure 6.7. The results were good enough to authenticate the parameters mentioned in the literature; the strategy to implement the selected deposition rate of 0.05 nm/s and to use the temperature of 400 °C for 1 hour was a good head start for the fabricating ITO

films which were at least transparent. The conductivity or the resistance of the film were not as yet measured properly, however as a preliminary observation the resistance of the sheet was measured with a digital multimeter at two fixed points on the film. Even though the readings of the multimeter always differed, but that is expected since the resistance is dependent on the distance between the probes, which differed as well. However, the readings always fluctuated between 100-85 Ω for this process run.

Sadly, after the second deposition and annealing experiment the hotplate of the lab malfunctioned and was decommissioned for repairs. The rest of the annealing experiments were thus done in a furnace which could provide temperatures more than 600 °C. After the second experiments, a series of annealing experiments were conducted at different temperatures ranging from 350-600 °C varying by 50 °C, all of which had good clear and transparent results. However, the colours of the annealed films differed with change in the temperature, amount of oxygen during annealing and the composition of In_2O_3/SnO_2 granules [4].

It is worth mentioning that the ITO granules used in the crucible for deposition process come in different compositions commercially. This has been discussed in Chapter 3 exclusively, the compositions of In_2O_3/SnO_2 used in the study were 90/10 and 95/5. Most of our study was done with 90/10, as in the beginning this was the only composition available in the lab. Later on, after the availability of 95/5 composition very little experimentation was carried out. The reason for that was, 95/5 composition has better transparency and has very little colour tinge in the film, however the sheet resistance was much higher compared to the ones observed with 90/10 granules. The sheet resistances of 95/5 were observed 10 times higher than that of 90/10 composition granules, after deposition and annealing. Figure 6.8 shows the colour difference at different annealing temperatures with 90/10 and 95/5 compositions.

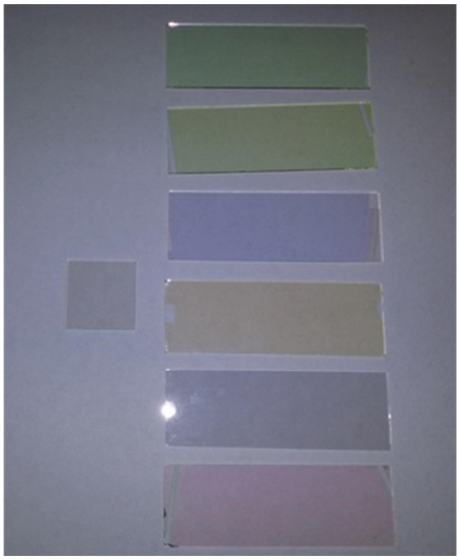

Figure 6.8: *Sample of 200 nm ITO films over glass slides with their corresponding annealing temperatures and composition of ITO granules.*

6.4 Transparency Measurements

6.4.1 Using Ocean Optics Jaz 350 Spectrometer

Although on the first glance after the deposition of an as-deposited ITO film an observer can never believe that the same film could become quite transparent after annealing. But the real question is how much is the film actually transparent? The transparency of the film is of prime importance for this study since the main aim was to fabricate microelectrodes that are transparent so they don't owe any obscurity of the cells when being viewed during the measurement procedures. Thus for measuring the transparency of the film a good quality spectrometer was used in the department. The spectrometer is the Ocean Optics Jaz 350 Spectrometer which is capable Vis-NIR measurements from 350-1000 nm. The device is fairly portable and modular; it has a halogen light source thus the mentioned spectral range. The modules include: a light source module, a sample holding module and a Jazz controller module that controls the halogen light source. The Jazz controller module measures the spectrum and relays the information to a PC via USB connection. The data received by the computer for analysis and the controlling parameters of the Jazz controller are all viewed and utilized by an interface software that comes with the device. The software manipulates the results into graphs and also manipulates settings for calibration of the device. The sample holding module of the device was designed and manufactured to hold transparent plastic cuvettes for absorbance test measurements of chemicals. However, for the transparency measurements for glass slide there were slits present in the same space. This allowed the glass slides to be loaded as well but they needed some support to remain at a vertical position relative to the base of the holder for no refraction and reflection from the light source. To provide that support some compressible packing material was used to fill the slits after placing the slides in them, this fastened the slides to the desired normal position to the base. The device had to be calibrated every time to compensate for the stray light in the background in both modes; with the light source on and with the light source off.

6.4.2 Reference Measurements of Clear Glass Slides and Air

Once the device was calibrated measurements for the transparency of the films was done. Since the primary interest was in determining the transparency of the film, the transparency measurements of the film without the glass slide was impossible as it was the substrate. So any measurements of the transparency would include the absorbance of light due to the substrate as well, which in this case is the glass slide. Logically the first step was then to measure the transparency of a clean glass slide without the ITO coating. For that a glass slide from the cleaned batch was taken and measured with the spectrometer. The clean glass slide was among the batch of slides that were cleaned using the same glass cleaning protocol that was discussed in the section 6.2. To make things systematic, every time glass slides were cleaned for deposition, one or two glass slides

were cleaned extra in each batch for measuring the transparency of the glass slide alone. The glass slides were measured and they yielded a transparency of 93 % almost every time even though the manufacturer prescribed value was 91.5 % the result was very close since the measurement were done in dark to avoid contamination from stray light, thus the difference of 1.5 %. The figure 6.9 can show the transmission of a clean and clear glass slide compared to air. The transmission through the glass was measured to be 93 % and 100 % through air.

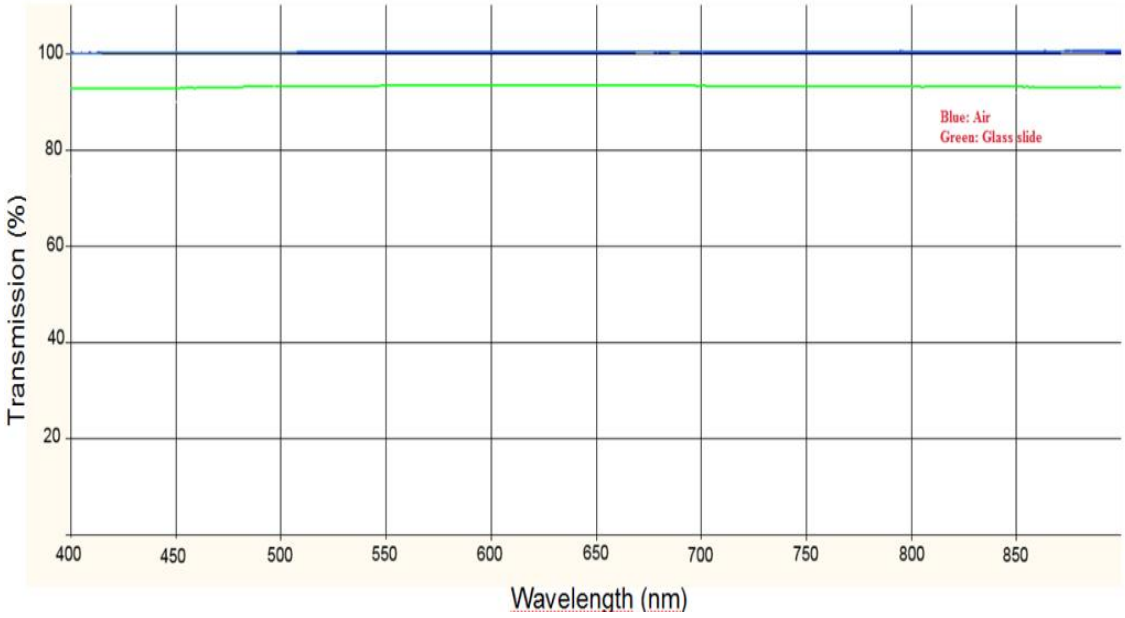

Figure 6.9: *Transparency measurements of a clean glass slide by the spectrometer.*

6.4.3 Transparency Measurements of as-deposited ITO Film

The next measurements were done for ITO coated slides with the same conditions. The first measurement was done for as-deposited ITO film on glass slide. The as-deposited slide is already shown previously in Figure 6.3 and with this black opaque layer the measurement was found to vary from 3 % to 10 % in visible spectrum and can be seen in Figure 6.10. An important point to notice here as well is that the figure also shows measurement of air and glass slide along with the measurement of the as-deposited ITO film. This helps understand with a clearer perspective as these two references are there in the figure as well, as mentioned already the transmission at any wavelength also has the deficit due to glass as well. As an example from Figure 6.10 of the as-deposited film spectrum, if we take the transparency of the as-deposited film at 650 nm which is approximately 10 % relative to air, it can be understood that there is still a deficit of transmission from the glass and that the actual transmission of the ITO as-deposited layer is more than 10 %. In order to deduce the actual transmission the 10 % has to be divided by 93 % to see what is the real transmission which would be relative to air in the end. The equation below can help understand the entire phenomenon:

$$film\ transmission \times 93\ \% = 10$$

$$film\ transmission = \frac{10}{0.93}$$

$$film\ transmission \cong 10.8\ \%$$

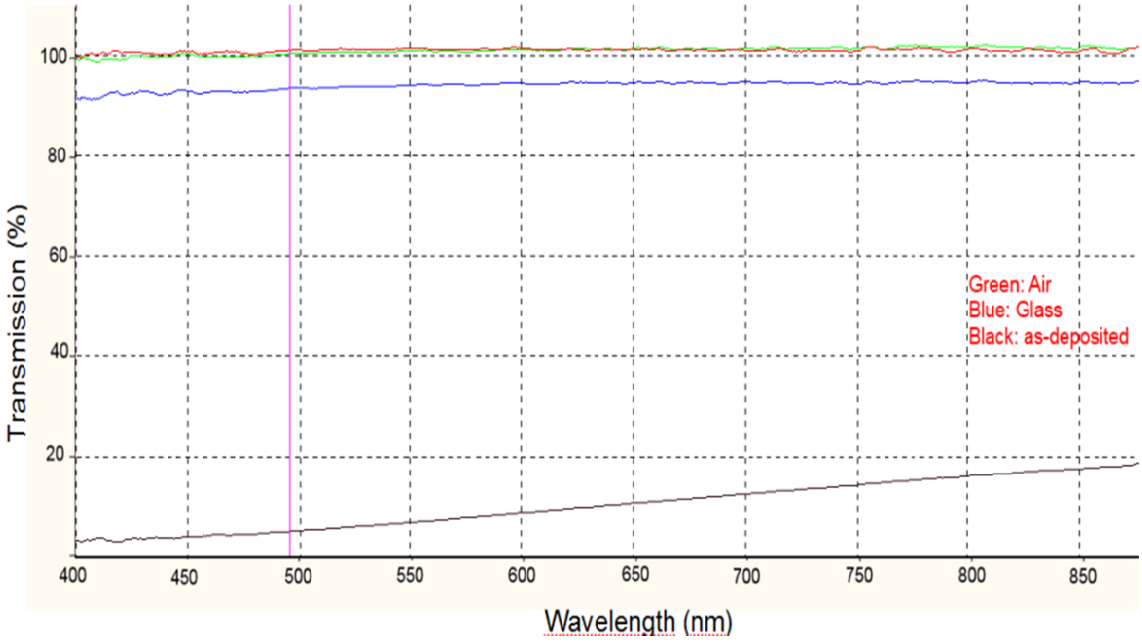

Figure 6.10: *Transparency measurements of as-deposited ITO film on clean glass slide.*

Thus the real (absolute) transparency of the as-deposited film (relative to air) at 650 nm wavelength was found to be 10.8 % instead of 10 %. Relating to this all the transparency measurements were therefore done having both air and glass measurements as well.

6.4.4 Transparency Measurements of Annealed ITO Films

The annealing process required the as-deposited thin films over the glass slides, be subjected to high temperature exposure in presence of air. To study the annealing effects on the transparency of the ITO films post annealing, the thickness of all the samples were set 200 nm, with deposition rate as 0.05 nm/s and annealing time of 1 hour. The study was conducted for a range of 300-550 °C and interval for annealing temperature was at first considered for 50 °C step change. However, 300 °C and 350 °C annealed films for 1 hour were not very transparent, so they were eliminated from the study initially and for the rest 50 °C increment did not bring about a very clear distinction. Thus the step size changed to 100 °C increment and studies for 300, 400 and 500 °C were investigated.

1. **300 °C Annealed Films**

The first annealing result of ITO film at 300 °C was measured and was observes as extremely non-transparent, same was the case with 350 °C temperature annealing process. So the study was automatically progressed to investigate 400 °C temperature. However later another annealing process for 300 °C was conducted on the evidence of a prior study from J.Zhou et. al which showed good results if the annealing time was increased to 18 hours or more [23]. Thus an annealing process at 300 °C was conducted exclusively and is shown in Figure 6.11. The spectrum measured the highest transmission within the visible wavelength at 617 nm with transmission of 90.7 %, surprisingly this result was observed higher than that off the literature. Since the application will deal with visible light spectrum, with light sources such as tungsten halogen (TH) light sources, that emit a continuous spectrum of light ranging from about 300-1400 nm. However, majority of the wavelength intensity is centred in the middle of the spectrum, ranging of 600-850 nm region. Thus transparency measurement values beyond 850 nm don't really concern this study for that matter. The least value of % transmission for this sample is observed at 723 nm for 83.4 %. Thus the average transmission value for this sample in the operational wavelength range is 87.1 %. Of course this transmission still has the attenuation due to the glass slide and if that is taken away the absolute transparency of the pure ITO film comes out to be 93.7 % transparency. Though the results seem more than satisfactory, the only drawback with this annealing process and result was, that the annealing time for 300 °C annealing was set for 24 hours. The annealing was neither carried out in a furnace nor on a hot plate, contrarily the annealing was done in a home oven. The reason for that was that such a long usage of furnace or hot plate was deemed unsafe and impractical to use and monitor.

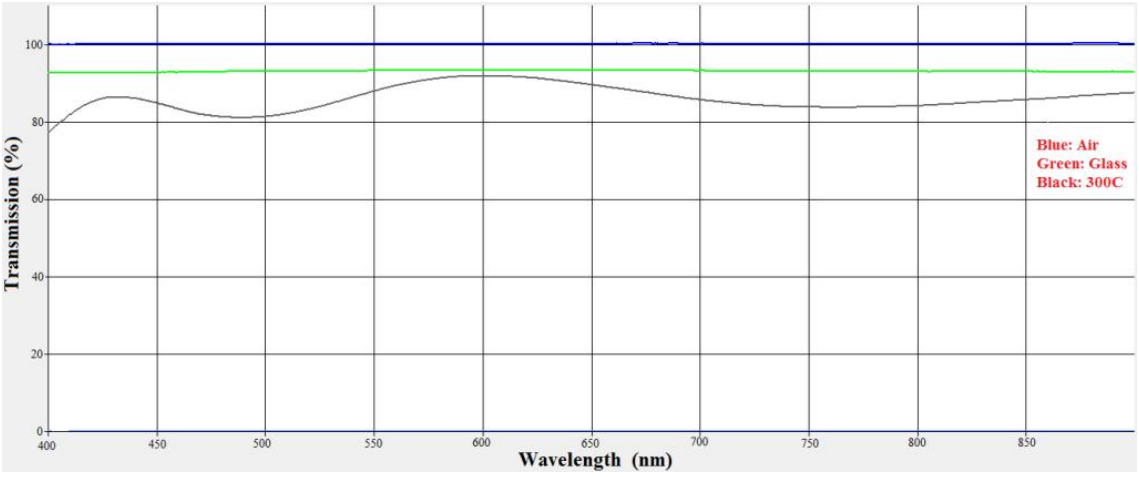

Figure 6.11: *Transparency measurements of 300 °C annealed ITO film.*

2. **400 °C Annealed Films**

The first annealing result of ITO film at 400 °C was also measured and is shown in figure 6.12, which measured two high transmissions within the visible wavelength. The

first one measured at 465 nm of 90.1 % and the second which was even higher, measured transmission at 820 nm of 92.8 %. Since the interest lies in values between 600-850 nm, the 820 nm result was astounding. The least value was observed at 600 nm which resulted in 82.3 % transmission, thus the average % transmission within the desired wavelength range resulted to be approximately 87.6 %. The absolute value of this average transparency of the ITO film alone was calculated to be approximately 94.2 %. Even this result surpassed the referred literature [8-9]. Even though the least value of transparency measured was 82.3 % at 600 nm, the important point to understand is that the total transparency for ITO base microelectrode will not be less than 82.3 % in this case. This confirmed two things; a) The use of a hot plate was just as effective, rather more suitable since the hotplate used in the experiment was in clean room and b) the direction was right in terms of deposition rate and cleaning protocol as well. After this measurement the expectations for 500 °C annealing rose high and looked promising.

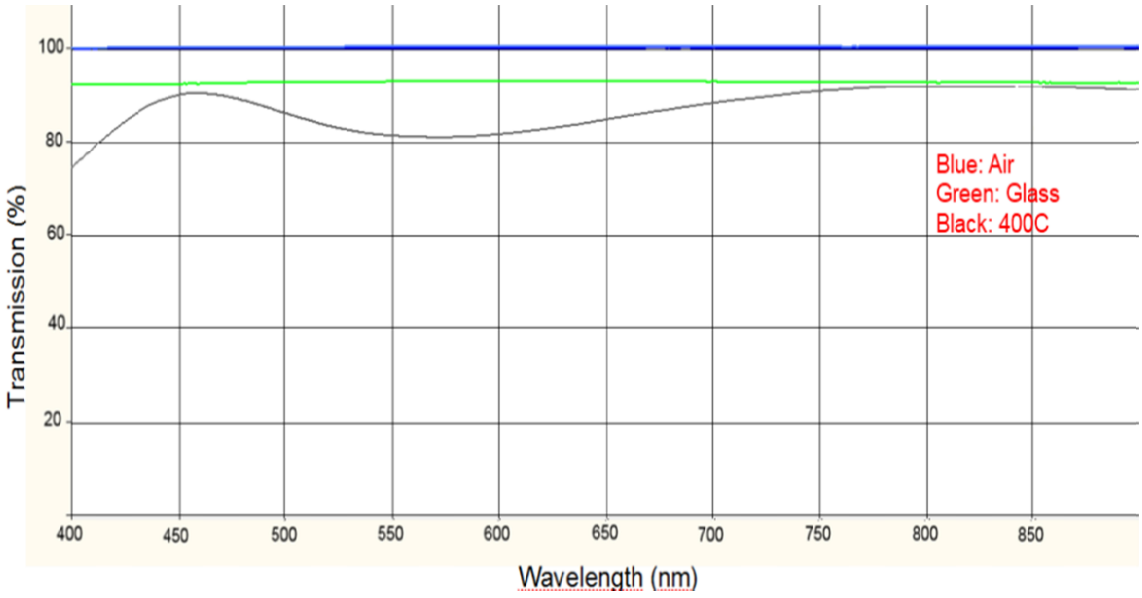

Figure 6.12: *Transparency measurements of 400 °C annealed ITO film.*

3. 500 °C Annealed Films

The result of a 500 °C annealed film was measured next the result of the measurement is shown in Figure 6.13 below and resemble quite a lot like Figure 6.12 result of 400 °C annealed film.

In the spectrum analysis of 500 °C annealed ITO film the first high transparency measurement was about 88.9 % at 438 nm in the visible range and consecutively 92.6 % at 750 nm. The lowest value measure was 83.2 % at the wavelength of 600 nm relative to air. The average transparency for this sample was calculated to be 87.9 % transmissivity. Consequently the absolute transparency measurement for the ITO film of 500 °C annealed sample approximated to 94.5 % transparency. Again the important thing is that

the transparency never falls short of 83 % in general which is a good result when considering transparent microelectrode.

An edge to 500 °C annealed film compared to 400 °C annealed film is that the highest transparency is also right in the middle of the visible range and the desired operational range of the TH light sources. Likewise, the least transparency measured was also 83 %, higher than the lowest transparency in 400 °C, which was 82 % even though the latter isn't too big of a difference but is still an advantage. To see more clearly the effect of annealing on the transmission spectrum of the ITO film, Figure 6.14 gives an elaborate illustration of comparison amongst the temperature steps of 300, 400 and 500 °C for annealing.

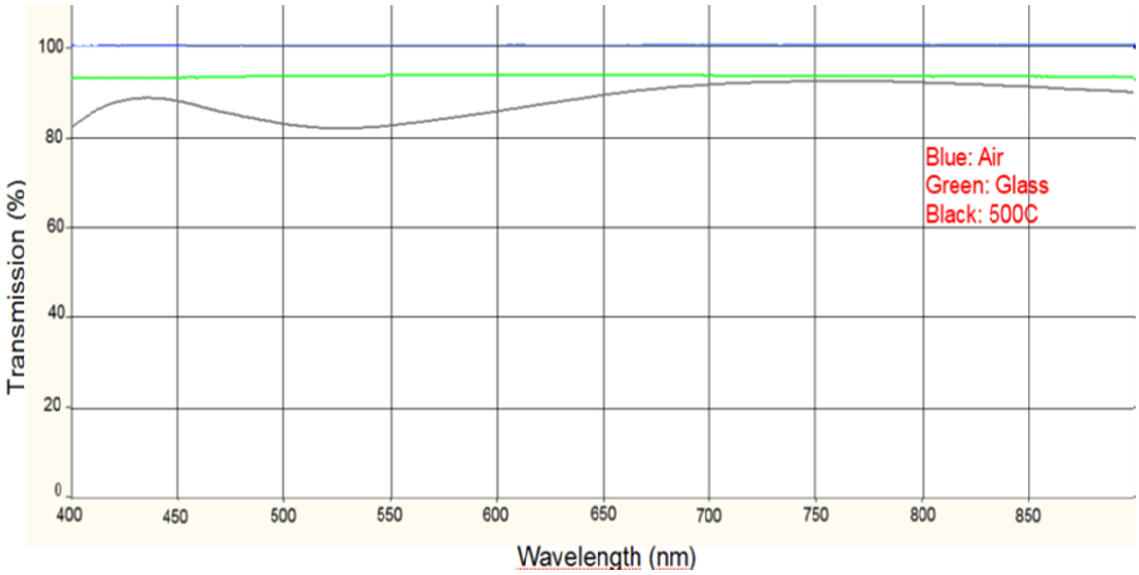

Figure 6.13: *Transparency measurements of 500 °C annealed ITO film.*

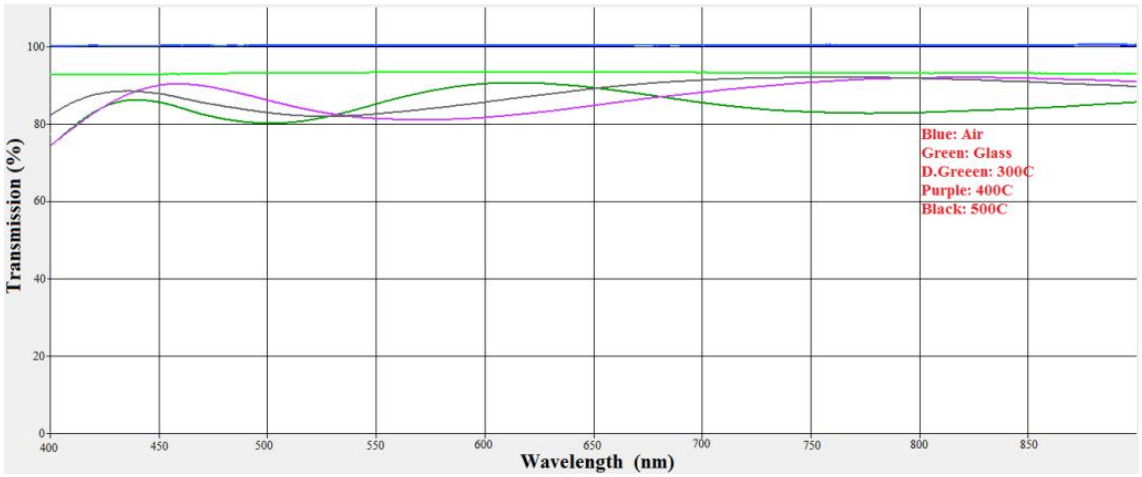

Figure 6.14: *Comparison between different temperatures of annealing on ITO thin film.*

6.5 Sheet Resistance Measurements

Sheet resistance measurements were the most important measurements for characterizing the ITO thin films to be suitable for microelectrode fabrication. The sheet resistance calculations were made using resistance measurements made with 4 probe resistance measuring method, illustrated in Figure 6.15. The resistance measurements are shown in Table 2. The measurements were done from the same ITO coated glass slides, as the ones used for transparency measurement. The dimensions of the glass slides were found as 76 x 26 x 1 mm (D x W X H) from the datasheet of the manufacturer [24]. Using these dimensions and the formula given below the sheet resistances for all corresponding resistances in Table 2, were measured.

$$R_s = R\frac{W}{L}$$

where

R_s: Sheet Resistance

R: Bulk Resistance (measured by 4 probe method)

L: Length of glass slide (76 mm)

W: Width of glass slide (26 mm)

The sheet resistance values (the 4th column) of Table 2 were calculated utilising the equation, constants and variables described in the column 3 of Table 2. The 4th column was derived for the sheet resistance for all the ITO covered glass specimens with different annealing temperatures. The results of sheet resistance values also surpassed expectations, from the literature review thermally deposited ITO and e-beam depositions should yield below 50 Ω/sq and all results were better than the benchmark. From Table 2 it is evident that the best result was yielded by 300 °C annealing for 24 hours. However, since the possibility for having an annealing time this long was out of the question that left the options of 1 hour annealing processes to choose from. Amongst theses the best result was obviously 400 °C annealing temperature. Though this result is peculiar since it was expected that 500 °C annealing should have yielded better results, but that wasn't the case for this study oddly.

Table 2. *Sheet Resistances calculated from bulk resistances in Table 2 to the corresponding annealing temperatures.*

TEMPERATURE °C	TIME (hours)	RESISTANCE (Ω)	SHEET RESISTANCE (Ω/sq)
500	1	132.3	45.1816
400	1	104.7	35.8184
300	1	180.1	61.6132
300	18	100.0	34.2105
300	24	37.6	12.8632

Having looked over the results of both sheet resistances and transparency measurements, it was decided to choose 400 °C as the annealing temperature as standard practice for annealing ITO thin films. Even though annealing at 500 °C showed better results for transparency measurements, the choice of 400 °C annealing was favoured because sheet resistance values would eventually play a more important role in designing better quality electrodes. Also the difference in sheet resistance values was much distinguished compared to the transparency measurements.

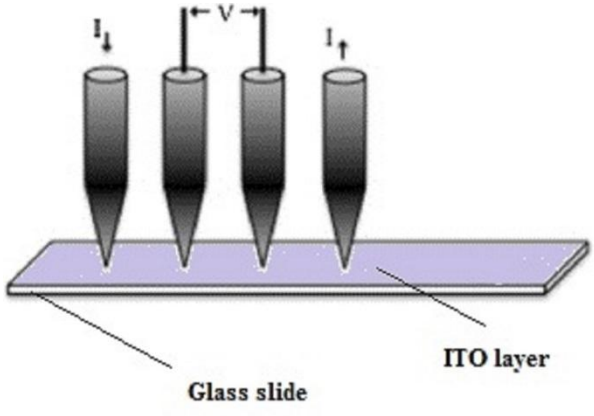

Figure 6.15: *A 4-probe measuring concept of the annealed ITO layer over microscope glass slide with equidistant placement of probes [36].*

7. TIER II: PATTERNING THE ITO FLIM

After the fabrication for ITO film was optimized for best transparencies and sheet resistances, the next challenge was to pattern it into the MEA layout. The patterning or micro-processing of the ITO into the desired MEA layout required to figure out optimum methodology to get rid of excess ITO from the glass wafers except the pattern needed, without causing the pattern to be affected. ITO can be patterned using etching and photolithographic techniques. The challenge remains to be able to pattern micro scale objects of ITO, making sure that the geometric integrity of the object does not deter. Photolithographic techniques become tedious and highly precise when the scale is reduced to micro or nanometres and there are more chances that the patterns might not be as accurate and precise with the slightest deviation or negligence.

7.1 Photolithographic Processes

All the necessary theoretical knowledge of the photolithographic processes needed to understand the experimental part is already explained in Chapter 5 of the document. The photolithographic process required in the study was needed to pattern the ITO thin films developed earlier. The main challenge in this part of the study was the patterning of ITO. This was generally known to be more common with wet etching using strong acids or bases. However wet etching for ITO, generally is suitable for patterns in the range of millimetres whereas the MEAs have geometric patterns as small as 20 μm at certain places. [28]

In the beginning it was decided to test patterning the ITO with wet etching using hydrofluoric acid (HF) and hydrochloric acid (HCl) as the prime etchants. The photolithographic process would have to be accordingly and the choices of materials henceforth were determined likewise. The resist chosen was PRI-2000A, which is a reddish maroon coloured positive photoresist to be applied over the ITO film layers. As opposed to the resist being viewable for transparent layers or substrates, it was also practically tested in the past. The developing solution or the developer of the resist was chosen as RD-6 developer, because it is a compliable developer for the resist. The spin coater was used to uniformly distribute the resist and it was set to rotate at 3000 rpm for 60 seconds. The exposure device used was a semi-automatic mask aligner and exposure device.

The photolithographic procedure was initially applied with everything according to the specific instructions of use e.g. it is mentioned in the manual for RD-6 developer to be used for thirty seconds after the exposure of 30 seconds. However, practically these and

many other parameter of use, always change according to the condition in the clean room and need to be tweaked to the users satisfaction and better judgment. The photolithographic process for fabricating ITO MEAs was actually tried, tested and optimized with the design of a flow-sensor developed in house by Mr. Tomi Ryynänen. The prototyping the flow sensor design instead of the MEA itself was to avoid wastage. Since the flow sensor is a quarter of a size of the MEA design with similar smallest dimension geometries, it yielded lesser wastage while perfecting the technique. Finally when the process was fully optimized it was employed for fabricating ITO MEAs. Figure 7.1 shows the picture of an ITO patterned flow sensor.

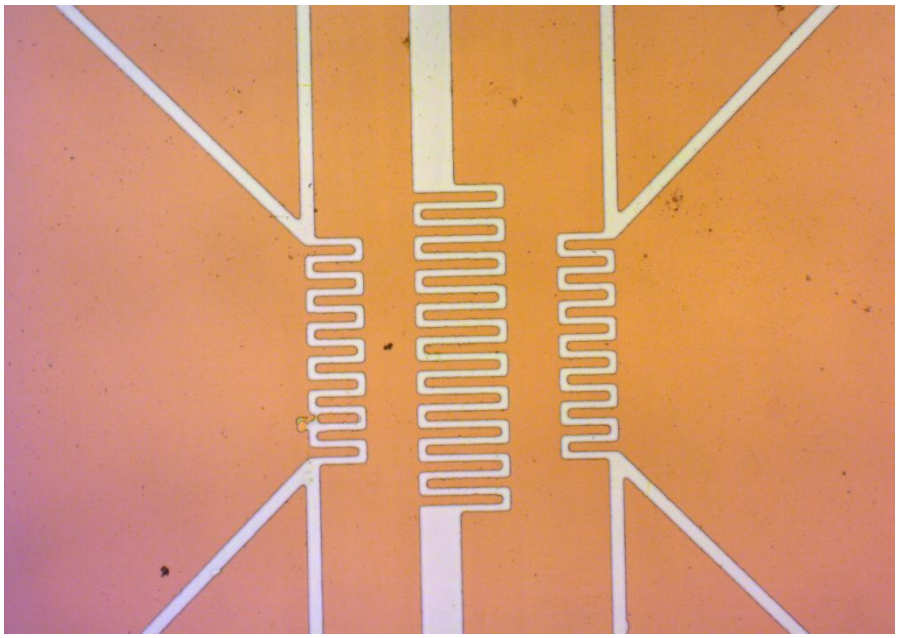

Figure 7.1: *A successfully patterned transparent ITO flow sensor prepared via dry etching and photolithography.*

The process always starts with the proper cleaning of the substrate, which in this case was the ITO covered glass wafer. The cleaning protocol was the same one used for cleaning the glass wafers prior to ITO deposition explained in subsection 6.2 except the final oxygen plasma was not used because it could affect the characteristics of the ITO. The resist application followed immediately after the cleaning protocol. The wafers were not subjected to an initial bake as mentioned in the theoretical part of the document; to drive off any excess moisture instead nitrogen was used to drive of any liquid or viewable moisture. The wafer was then mounted on the spin coater and sufficient resist was poured using droppers very carefully not to over spill or under use as it affected the uniformity of the resist layer after the spin. The spin was set to be at 3000 rpm for 60 seconds, after the resist was poured on to the ITO layer. After the spin the wafer was inspected to see if the resist layer was uniform and without any bumps and ridges. If there would be any imperfections after the spin coat the wafer would go

through the cleaning procedure again and then the photoresist would be poured all over again followed by the spin. Once the spin was over, the wafers with the resist layer were subjected to a bake of 120 °C for 1 minute. After which the wafer was subjected to the mask aligner and exposure device. In this device the first step was to load the proper photo mask of the desired pattern that needs to be impressed upon the resist layer. Then the wafer with the pre baked layer is loaded in the substrate chamber and aligned properly with the mask. Once the alignment is properly optimized and the contact between mask and resist layer is sealed the exposure is allowed. The exposure in this case was initially kept for 30 seconds, which later on was optimized to 25 seconds. After the exposure, came the step for developing the required pattern using the developer, which in this case was RD-6. This post exposure, resist development, was done using for 30 seconds in the beginning but later was optimized to 45 seconds due to the change with exposure time. The next step was hard baking, which was done at 130 °C for 1 minute after the developing. It is important to observe here that the best exposure requires optimization of these two parameters essentially. After the developing and the baking of theresist of the wafer it is subjected to thorough washing with DI water to avoid any extra and unnecessary development process that could alter the geometric dimensions of the impression required. Once thoroughly washed the developed layer of the ITO is then subject to post development bake at 130 °C for 1 minute. Now, the wafer is good to go for etching in the exposed resist parts.

This entire iteration is done similarly every time when a new layer is introduced over the glass wafer. After etching the resist needs to be stripped from the underlying ITO layer on the glass wafer. This is done by simply placing the wafer in excess acetone for a minute or more and washed with DI water and subjected to the cleaning protocol once more. In the end the final product is an ITO patterned in shape of MEAs on the glass wafer. This is in no way the end of the fabrication process for fabricating MEAs; the patterned wafer is once again subjected to deposition of a silicon nitride (Si_3N_4) isolation layer. This isolation layer is again required to be patterned so as to cover the entire wafer above the ITO patterned MEA but only to expose the electrodes and the contact pads. Thus another iteration of photolithography is required except this time a different photo mask will be used for a different impression over the post bake resist, rest all the iteration remains the same.

7.2 Wet and Dry Etching

In section 7.1 it is mentioned that the photolithographic process was optimized first to fabricate a smaller flow sensor, the same was the case for the etching process. The etching technique was first tried, tested and optimized for the flow sensor as well. Actually it was the etching phase of the study that took the most time and laborious research to nail the optimum methodology for the fabrication of the ITO standard MEAs. Literature review in the beginning pointed out to follow for wet etching to pattern ITO films, using

acids like hydrofluoric acid (HF), hydrochloric acid (HCl), nitric acid (HNO_3) and their mixtures like aqua regia [25-27] etc. However, the wet etching mechanism chosen for this study on the basis of literature review did not yield any successful results and were deemed total failures. So the focus shifted to dry etching using RIE, as it was already available in the clean room of the department. It was found that ion milling using plasma and argon ions was an alternative for patterning ITO thin films for micro patterns [28]. Using the dry etching a successful pattern of flow sensor was developed and was then used for fabricating the ITO MEAs.

7.2.1 Wet Etching Experiments

The very first attempt to etch the layout of the flow sensor from an ITO film covered on a glass wafer was done using diluted HCl alone. The maximum strength of HCl available was 60 %, which meant that for every 100 ml of the solution in the bottle 60 ml was HCl or H^+ & Cl^- ions and 40 ml was distilled water. So for the first experiment it was decided to use a very dilute solution of 1:10, meaning 1 part HCl and 10 parts water (10 ml HCl and 90 ml water). With this concentration the etching rate was so slow that even after half an hour the ITO layer was still not etched but the surface had started disintegrating and becoming flaky. After 65 mins, the experiment was aborted as the etch rate for this kind of solution was approximated as 10 nm per minute and the thickness of the ITO film was 250 nm so the expected time for etching was around half an hour. After 60 minutes, double the time had passed and still the surface seemed intact, so the experiment had to be aborted. For the next experiment a more concentrated solution was used where the ratio was set as 1:3 of the acid to water. In this experiment again the thickness of the film of ITO was 250 nm, and this time the film was immersed for 20 minutes, at first while still agitating the solution. During this trial the ITO's surface began to disintegrate after only 3 minutes, upon this it seemed for the time being that the solution was etching according to the etch rate mentioned for the last solution ratio. However, after 20 minutes when the glass wafer was washed with water and inspected under the microscope the pattern had been destroyed as well. The smallest patterns in the entire layout has been etched away as well, so another trial was attempted with similar conditions, but this time the wafer was taken out of the etchant after 6 minutes only. Upon washing the glass wafer and inspecting under the microscope it was found that the layout of the flow sensor was intact. Thus the resist was striped using acetone, and washed properly and then inspected again under the microscope, the result was a failure again. The etchant seemed to have seeped under the resist due to the isotropic action that happens in the wet etching. Another trial was thought to be given a go, but this time the concentration was decided to be slightly lower compared to the last time. So in this attempt the ratio was set for 1:5; one part acid, 5 parts water, the thickness was the same again. The glass wafer with the ITO was placed in and after 4 minutes and 30 seconds the surface began to flake, and after 8 minutes it was taken out, washed and inspected under the microscope. Upon viewing it under the microscope the pattern seemed intact with the photo-

resist so the resist was again striped washed, and viewed again under the microscope. This time again, the smaller patterns of 10 microns were destroyed even though there was still ITO in the peripheries of the exposed parts of the wafer.

The solution with HCl and water alone didn't seem to work so a new etchant recipe was tried where HNO_3 was introduced in the aqueous HCl solution and is also known famously as "aqua regia" [25]. For the first trial of this experiment the ration chosen was 1:3:10, where one part is HNO_3, three parts are HCl and 10 parts of DI water. Again for this trial the thickness of the ITO film was also 250 nm, the film was dipped in the solution and even after 15 minutes there was no surface flaking as it happens when the etching begins. After 20 min of dipping, the surface began to flake and by this time it was realized that the solution was perhaps too dilute. The next trial for this solution had the ratio modified to 1:3:5, where the water was now reduced from 10 parts to 5 parts. In this trial the surface disintegration occurred just after 1 minute and the ITO seemed to have vanished in 3 minutes, after 3 minutes the wafer was inspected with the resist on and the resist had broken patterns at the smallest object in the layout of the flow sensor. The etchant seemed to have been slightly more concentrated so the solution ratio was again changed and this time the water was increased from 5 parts to 7 parts, giving a final ratio of 1:3:7. In this trial as well the thickness was the same as in all the previous trials and the first sign of flaking occurred at 5 minutes. After 7 minutes the wafer was pulled out and the inspected under the microscope there were many patches of semi etched ITO still in the peripheral exposed areas other than the layout, however the smallest patterns of 10 microns were still damaged even though all the stray ITO had yet to be etched way. Upon such a result it was again considered that this etchant solution was also an utter failure, so a new recipe of a more suitable etchant was needed to be tried and tested.

After a little more researching for possible ITO etchants, another recipe utilizing HF, H_2O_2 and water was found and known to be a possible etchant. It too was given a series of trials as well. For this recipe the suggested ratio of mixture was described as 1:1:10 and the etch rate was also estimated as 12.5 nm/s. Even with this recipe the results were not satisfactory in the least bit. The etchant would take too long to etch away the residual layer of ITO of the exposed surface, by which time the etchant would seemingly seep underneath the mask and destroy the microstructures intended to remain un-etched.

It was somewhat clear that the wet etching owes a steeper bias than expected, with the thickness of layers being dealt with, for this study. At higher thicknesses (300 nm and above) of ITO layer the etchant seemed to be seeping under the mask no matter what type of recipe was used. Some would take longer than others but eventually all the wet etchants eventually had the similar effect, degrading the pattern once the etching of the residual surface layer completed. This was the last recipe used to test wet etching and with its failure, it also sealed the possible fate for using wet etching as a microfabrication process for the preparation of our MEAs any further.

7.3 RIE Machine and Dry Etching Optimization

After having failed repeatedly at numerous wet etching iterations, it was time to consider alternative approaches for such as dry etching or lift off processes. In one of the literature review it was suggested that lift-off process for micro-processing the ITO layer wasn't an optimum choice and the results aren't always promising. The reason was that high velocity particles during the deposition process of the ITO penetrate through the cracks of the photoresist, which too are formed during the deposition. This causes washing of the resist difficult and sometimes impossible, rendering areas without ITO to have ITO particle [28]. So it seemed that a better choice for micro-processing would be dry etching/plasma etching.

When it came to dry etching more than one recipe was found which had different gases and sometimes a mixture of different gases used as etchants. The only consideration here was again using the gases available in our RIE device. Thus a lot many choices were altogether dismissed owing to the unavailability of certain gases suggested in literature. An educated guess of using recipe with only a single gas as etchant seemed like a sensible idea, as lesser variables would come into play. Thus a single and the very first reference by Shabir et al paved way for experimentation for dry etching [28]. This method for dry etching utilized only argon in plasma for etching the ITO away. Since it was dry etching and that too in RIE device the result was expected to be highly anisotropic unlike in the wet etching experiments. The process involved etching ITO using argon atoms in plasma, where in the argon atoms would physically knock out the ITO molecules from the glass substrate. Unlike other mechanisms of etching where chemical changes causes etching this process is rather a physical one and can be referred to as ion milling [28].

When using the RIE device for etching, a few things need to be kept into consideration beforehand. The parameters of dry etching through RIE need a proper understanding of the kind of gases used, then their corresponding pressures that are required to be maintained in the chamber during the process and also their flow in and out of the chamber upon being used up during the procedure. Apart from optimizing the gas, other parameters need to be optimized as well for the plasma generation that includes choosing the appropriate RF (Radio Frequency) power and chamber pressure. Lastly, it isn't necessary that parameters for devices mentioned in the literature be valid or workable at all. The major reason for why the literature parameters do or do not work, is that each plasma device is unique and the parameters that work with one do not necessarily work with other device (even if they were of same model and brand).

Thus the recipe used for dry etching of the deposited ITO thin films was derived from the one followed in [28]. The working fully optimized recipe that was finally used for this study was based on the literature recipe but was only successful after many tweaks. Wherein, the RF power was set to 250 W, even though the recipe of the literature uses

100 W, the reason for that will be discussed shortly. The chamber pressure was initially maintained at $1x10^{-4}$ Torr, then argon was introduced in at a steady rate of 70 sccm (cm^3/min), causing the operational pressure to stay steady around 10-11 mTorr. The process takes around 75-80 minutes to etch away all the unrequired ITO from the glass wafer, leaving behind the photoresist and underneath the un-etched pattern of the ITO required. The pattern was found to be extremely anisotropic and yielded the perfect result as was expected. However, one minor inconvenience was observed, which was already known beforehand, the photoresist got burnt and was difficult to remove by just pouring over the acetone. Some physical agitation was needed to remove the burnt photoresist properly and completely, for that initially acetone dipped cleanroom cloth was used to gently scrub off the remains of unwashed photoresist from the acetone wash.

The recipe was not followed exactly as stated above, for the very first time during the pilot run. The above recipe, for dry etching was tweaked to its current optimum form by actually starting with all the parameters in [28]. According to the findings in Shabir et al, the initial pressure of the chamber is set to $1x10^{-4}$ Torr and then argon is lead to flow in at a steady rate in order to change the final pressure to 11 mTorr. However, no mention of the argon in flow was mentioned. The only mention of gas flow rate was that it should be as small as possible because at higher flow rates the ion milling efficiency of the argon gets attenuated due to inter collision of argon to argon, rather than argon to ITO [28]. Thus the argon flow rate had to be figured before beginning the actual etching. To do that, the empty chamber of the RIE device was pressurized at $1x10^{-4}$ Torr, with RF power set to 100 W, and then test runs were made to observe the least flow rate of argon that supported the desired chamber pressure for a complete run of 20 min. It was figured that 70 sccm of argon was the least flowrate that could run the etch cycle. Once the flow rate for argon was figured as 70 sccm, the next step was to run a pilot run to etch a small flow sensor to see if all the other parameters worked properly. According to the literature for dry etching 150 and 200 W RF powers were resulting in uncontrollable and unstable etch rates, to the extent that they report pinholes forming in the substrate at RF 200 W. For this reason, the very first run of the dry etching was also set with RF power of 100 W. However, it seemed to have no affect over the ITO layer what so ever, even after a serial run of 3 iterations each timing 20 minutes, thus resulting an overall etch time of 1 hour. Thus again using hit and trial method higher values of RF powers were tested and finally a value of 250 W RF power was observed for success. A visible change was noticed in the ITO film as it turned cloudy from transparent, along with a spike in the resistance value. Thus the same iteration of etching process with 250 W RF power and 70 sccm argon inflow was run again for 20 more minutes. After the second run, the ITO film's appearance changed to further densely clouded surface than before and the resistance value also elevated considerably. Successive iterations were made until the cloudy surface reappeared as transparent glass and a DMM showed unreadable resistance, to ensure all the unnecessary ITO was etched away. Finally, after a total of 4 iterations the flow sensor reassumed the transparent appearance of the glass

substrate from places where ITO was supposed to etch away and the DMM also showed unmeasurable resistance upon placing the probes at the same points.

Inspection under the microscope showed no defects in the pattern of the flow sensor and no undercut etching in the geometry of the flow sensor as well.

7.4 MEA Pattern of ITO Film

Once the dry etching with argon was optimized and perfected, the next step was to pattern the MEAs using the ITO films deposited and annealed on the glass wafers. For this the photolithographic process demanded masks in the layout of MEAs, the masks used for the standard 8 x 8 MEAs, were the film masks used with close contact mask exposure device. The mask layout was designed in house by Mr. Tomi Ryynänen, and there were two layouts used for 8 x 8 standard MEAs used and experimented in this study. Figure 7.2 shows the layout of 8 x 8 Standard MEA without a heat sensor, where the electrode diameter is 30 µm and the spacing between each adjacent microelectrode is 200 µm. Figure 7.3 shows the second layout of 8 x 8 Standard MEA with a temperature sensor in the middle, with electrode diameter 30 µm and the electrode spacing as 200 µm apart.

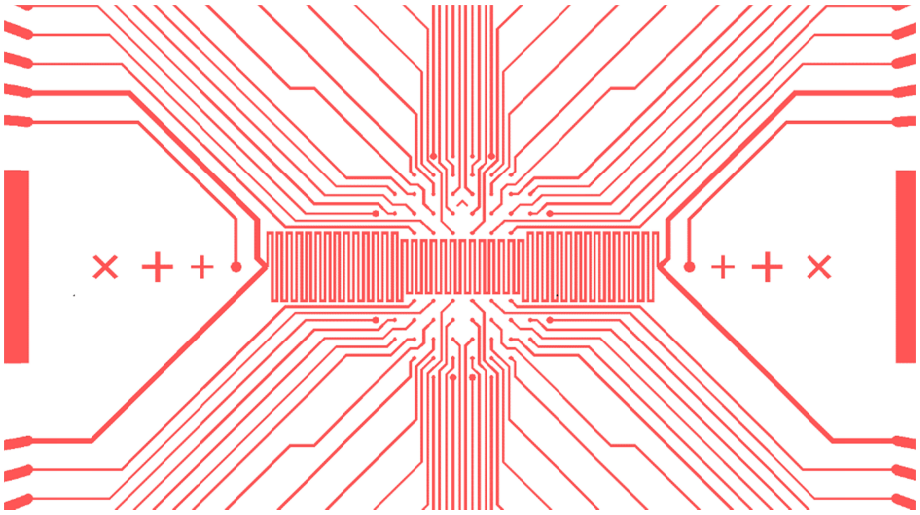

Figure 7.2: *Mask design of the Standard 8 x 8 MEA with heat sensor in the middle layout to be used in the mask exposure device for exposure with positive photoresist.*

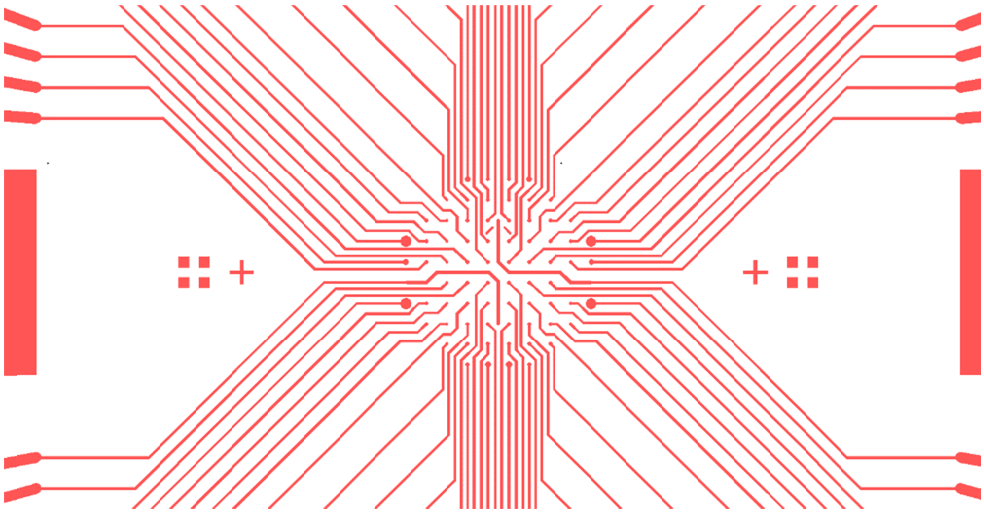

Figure 7.3: *Mask design of the Standard 8* x *8 MEA layout used in the mask exposure device for exposure with positive photoresist.*

The time period for the entire etching process of the MEAs into the MEA pattern from the ITO deposited glass wafers for the (MEA substrate) took 80 minutes for the very first batch of MEAs that were designed using wafers with ITO film thickness of 700 nm.

There were more masks used in the process of MEA fabrication, which included masks for pattering the Ti alignment marks and for patterning the exposed electrodes and contact pads with the Si_3N_4 insulation layer.

8. TIER III: MEA FABRICATION AND TESTING

After the first successful prototype flow sensor was developed shown in Figure 7.1, the second step in fabrication was complete. The first step was the fabrication of transparent conductive ITO thin films on glass substrate, the second step as mentioned was the patterning of the same ITO thin films into distinguishable micro-patterns. The third and the final tier of this thesis study involved, not only patterning the layout of the MEA from the thin ITO films but also to perform all the necessary tweaks and optimizations to fabricate working MEAs, which could measure the activity of beating cardiomyocytes. The second tier took most of this study's time, however the most work was cut out in tier three, as it required the processes and techniques to be tested again and again for the best results and also included the testing and measurements of the designed MEAs.

8.1 MEA Fabrication and Optimization of Microfabrication

Once a working recipe for argon dry etching in the RIE machine was finally discovered and tested, the next step was to use the same process to pattern the MEA layout from the film ITO. Since the flow sensor was successful in patterning using this process, so it was natural the process had to work for MEA layout as well. The only concern was that the MEA layout had electrode wirings that were as narrow as 20 μm and whether or not those structures would pattern out properly or not. So an initial or pilot run was made to confirm if the results were as successful as in the case of flow sensor. As expected, the results after the pilot run were just as successful and the 20 μm electrode wirings were holding their structural integrity and measured under the microscope to be just as such. The result of the dry etching to pattern the MEA layout of the ITO thin film for the very first time can be seen in the figure 8.1, the figure shows the snap of the MEA under the microscope at 5x zoom, the pattern is seen in pink colour while the glass wafer on which the pattern holds is seemingly brown colour in the background.

8.1.1 Initial Process Flow of Microfabrication

Before the process flow can be understood and decided for any MEA it is important to understand what key components MEAs possess. Usually standard MEAs have a glass substrate which holds upon it the entire MEA layout of a particular conductive thin film of metals or semiconductors, upon which is another transparent nonconductive isolation layer. So in short the simplest MEA should be a two-layer device, with electrodes wirings and contact pads as the first layer and on top of this layout the transparent nonconductive isolation layer which covers the whole MEA only to expose the individual elec-

trodes and the contact pads. In this thesis study the MEAs to be designed were 8 x 8 Standard MEA fabricated out of transparent ITO thin films, underneath an isolation layer thus a two-layer device and so the process flow was planned accordingly.

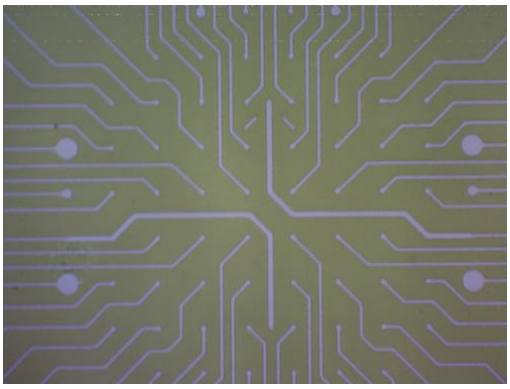

Figure 8.1: *Microscopic evidence of the successful patterning of ITO thin film into MEA using argon dry etching in the RIE device. The layout in pink is the ITO MEA layout on glass substrate (brown).*

The first prototypes followed a process flow of fabrication which was to fabricate ITO MEA layout over commercially manufactured glass wafers for MEA from Thermo Fisher Scientific Gerhard Menzel B.V. & Co. with dimension 49.0 mm x 49.0 mm x 1 mm. These wafers were first cleaned by the cleaning protocol used in the deposition part of the study mentioned in chapter 6, and will be used before each sub process of the microfabrication process flow. Next these glass wafers were put to ITO deposition through the metallization device or the (e-beam coater). Then the wafers were subject to 400 °C post annealing for 1 hour after the deposition. The wafers were once again subjected to cleaning protocol, before the process of photolithography for MEA patterning. The wafer, after the photolithography process, were put in the RIE device for argon dry etching for 80 minutes with all the parameters set according to the section 7.3. After the dry etching was complete the wafer were stripped of the photoresist using acetone wash and some wiping, and was subsequently subjected to the cleaning process once more. The wafer was now bearing the ITO MEA layout and was subjected to a 500 nm deposition of the isolation layer of Si_3N_4 (silicon nitride), discussed in the previous section, using PECVD (Plasma-enhanced chemical vapour deposition) method. The PECVD deposition of Si_3N_4 was done by another cleanroom team at the ORC (Optoelectronics Research Centre) at TUT. After the deposition of the Si_3N_4 isolation layer, the wafers were again subjected to the cleaning protocol as they had to be photolithographed for the second time to expose the individual 60 electrodes and the contact pads of the MEA. Once they were done with the second photolithography process, the wafers were again put in the RIE device for dry etching of the Si_3N_4 layer.

The only problem in this process flow came at the very end when the second set of photolithography was being done. The ITO alignment marks on the MEA, to which the film mask was to be aligned for the patterning of the Si_3N_4 layout could not be aligned

properly. The reason for that was the microscope of the mask aligner and the exposure device had an incandescent lamp without a needed filter. This caused the ITO alignment marks on the MEA, impossible to view and align with the mask for the Si3N4 patterning. Thus as a result the initial prototypes had a lot of miss alignment and the ITO electrodes on the MEA were not exposed properly so as to give electrodes with 30 µm diameter in most cases. Figure 8.2 clearly shows the misalignment of the ITO electrodes to the Si_3N_4 holes intended to expose the electrodes.

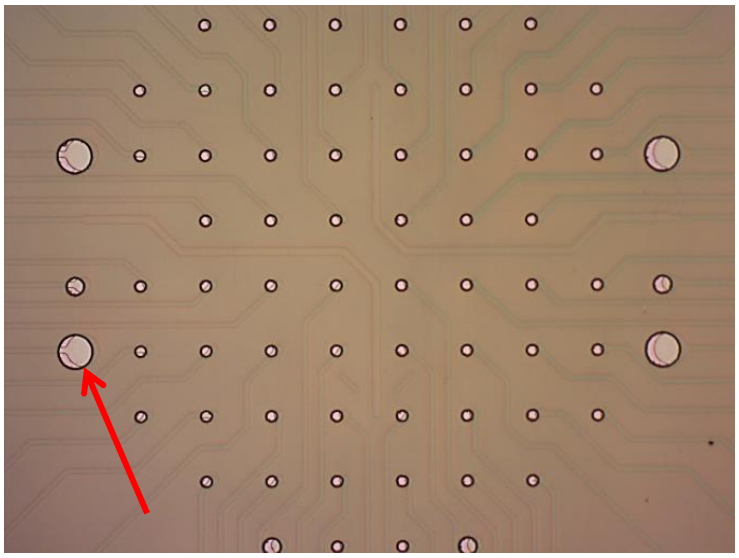

Figure 8.2: *Microscopic snap of the first prototype ITO MEA with isolation layer, horribly aligned due to lack of visibility of alignment marks during photolithography process. The arrow indicates to the misalignment.*

Table 4 shows a summary the initial process flow and can be understood by the followings steps.

Table 3. *Initial process flow summarized in steps*

1. Cleaning Protocol	
2. E- beam Deposition of ITO film, 500nm thickness	
3. Annealing at 400°C for 1hour	
4. Cleaning Protocol	
5. Photolithography 1 (for ITO patterning)	
6. ITO Dry Etching in RIE device for 80 mins.	
7. Stripping Photoresist and Cleaning Protocol	1st Layer
8. PECVD Deposition of Si_3N_4 (Isolation layer), thickness 500nm	
9. Cleaning Protocol	
10. Photolithography 2 (for Si_3N_4 patterning)	
11. Si_3N_4 Dry etching for 2.5 mins	
12. Stripping photoresist and final Cleaning Protocol	2nd Layer

Since the results of the initial process flow for the microfabrication of transparent ITO MEAs wasn't exactly up to the standard there was definitely some tweaking and optimizations required for the process flow to yield better results. For that the actual reason

of the shortcomings had to be reviewed and addressed consequently. The problem with the initial process flow was that the ITO alignment marks weren't visible on the mask aligner and exposure device's microscope. So a strategy had to be implemented in order to solve the viewing problem and eradicate the problem of misalignment once and for all. Hence a new process flow was developed to address the problem of misalignment of the different layers of the sensor.

8.1.2 Optimized Process Flow of Microfabrication

The misalignment in the ITO patterned layer and the Si_3N_4 patterning layer had devastating results of the initial prototypes. Therefore, to address them, it was decided to experiment by using opaque alignment marks. These alignment marks, would be fabricated by some other material altogether which was not only easy to deposit but also easy to pattern. Thus titanium was selected as the material of choice to fabricate the alignment marks. The only problem now was that the new process flow required the first thing after the very initial cleaning protocol was to deposit Ti rather than ITO. There were two good reasons for that; one the alignment marks are a kind of reference and therefore they have to be the first layer to be patterned so that all the subsequent layers would follow in alignments properly. Second, all the ITO covered wafers without the alignment marks were now rendered useless too, because if Ti was deposited over the ITO layer and then fabricated it would affect the ITO layer underneath. The Ti fabrication into alignment marks was to be done via an etching solution ($HF : H_2O_2 : H_2O$) as the etchant, which also etches the ITO so the underlying ITO layer would be etched to some extent.

Another surprising discovery was made related to the current dilemma during the time dry etching technique for ITO using argon was being studied. The discovery was that afore mentioned Ti etching solution, was found to be a very strong etchant with extremely high etching rate for Ti compared to ITO. It was learnt that if Ti was used to mask ITO rather than the photoresist in the photolithography process, and then Ti was patterned to the masking layout using wet etching, it might behave as a better photoresist than PRI-2000. However, it failed devastatingly, since a 200 nm thick Ti film deposited on bare glass substrate would completely etch within 30 seconds, but on top of ITO the Ti did not etch as expected. It took more than 3-4 minutes for the surface Ti to get removed. Upon removal the underlying ITO was damaged severely to an extent that the transparency of ITO was diminished majorly by forming a rather flaky surface of the ITO. This unfortunate failure was one of the bigger reasons why Ti deposition and patterning into alignment marks had to be one of the first steps in the new process flow.

With the inclusion of the Ti alignment marks as the first layer now, the MEAs got upgraded in design from being a two layer chip to being a three layer chip. Thus for a better understanding Table 5 explains the new step by step process flow of the microfabrication.

Table 4. *Step by step summary of the optimized process flow of microfabrication*

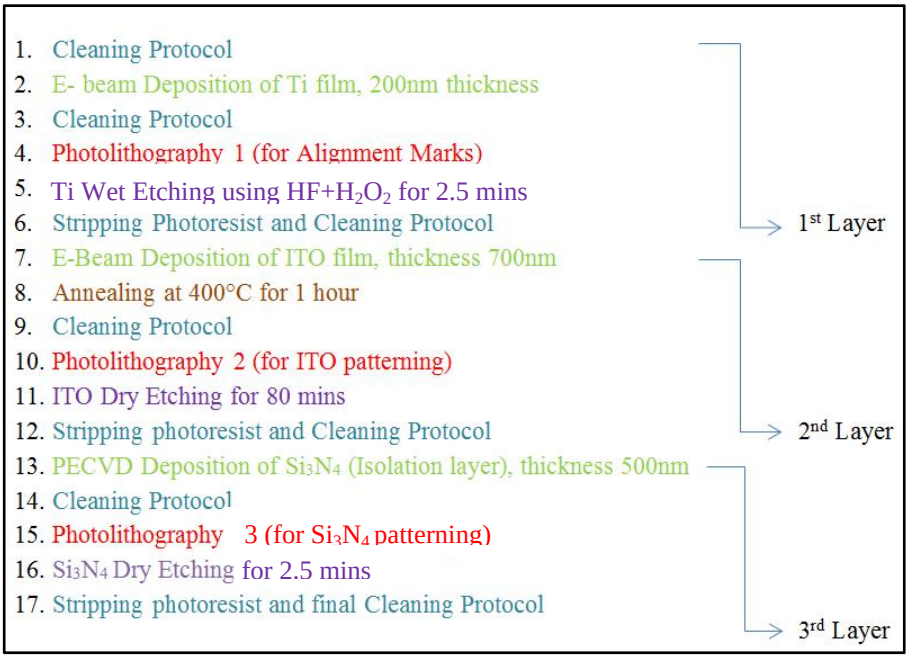

Comparing Tables 4 and 5, immediately the differences can be spotted which are addition of an extra layer in the biosensor and all the related sub processes for the layer. The Titanium layer in the beginning is deposited using the same metallization device used to deposit ITO. The deposited thickness for Ti was 200 nm as it was sufficient to create opaque structure on the wafer. Next it was subject to the cleaning protocol and then the first photolithography process for the fabrication of the alignment marks. After that the wafer was put in a (HF : H_2O_2 : H_2O) etchant for hardly 30 seconds and the Ti etching was complete. It might seem confusing in Table 5, mentioned 2.5 minutes for etching Ti but that is to ensure that entire Ti is removed properly. By using such an extra amount time it gets ensured that no stray Ti particles remain which may interfere with the MEA pattern. The removal of photoresist and cleaning protocol was employed and here onwards after Ti etching. The rest was absolutely the same as the initial process flow for fabrication of the MEA layout layer and the isolation layer.

The result of the new and optimized process flow was successfully patterned standard 8 x 8 Transparent ITO MEAs, which were now ready for testing before use and can be seen in Figure 8.3 in comparison with Pt standard 8 x 8 MEA.

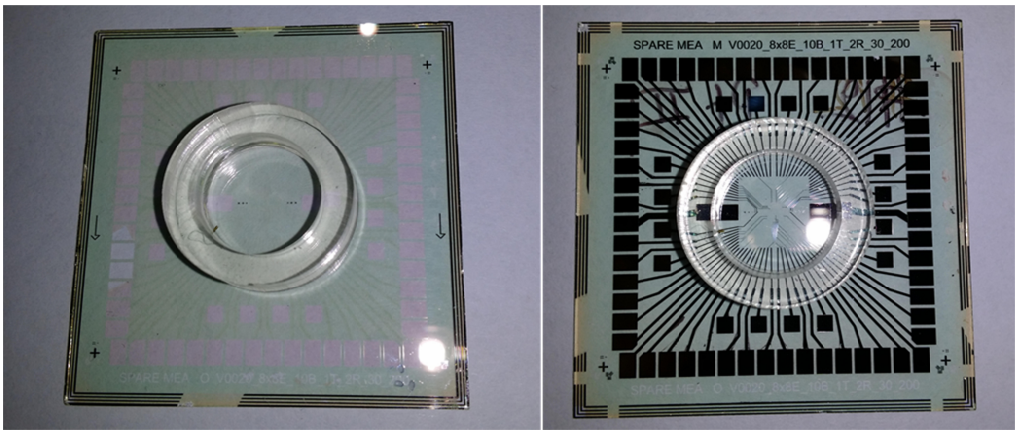

Figure 8.3: *On the left 8* x *8 Transparent ITO MEA compared to Pt MEA on the right.*

8.2 Testing the Fabricated MEA Prototypes

Once the process flow for the microfabrication was optimized and the first viable prototypes were designed and fabricated they were ready for testing to figure if they were actually functional rather than just look functional. The testing processes included for this study were the impedance measurement and the noise measurement. It is important to understand that there can be other characterization tests that can be performed to determine the further quality of the microelectrodes fabricated, these are mentioned elaborately in chapter 6. The reason for doing these two basic testing was, firstly we had no other testing facilities available in our own department and then these two are the most essential to comply the bare minimum testing requirements.

8.2.1 Impedance Measurement Testing

After being analysed visually under the microscope for physical defects in the structure of the geometry, the successful prototypes were subjected to impedance testing. For the impedance testing the MEAs first needed PDMS wells, which were so graciously provided by the Micro & Nanotechnology group of our department. Special credit goes to Mr Joose Kreutzer who was able to fabricate them for this study. The PDMS rings help to hold the culture medium during *in-vitro* measurements of the cells or tissues etc. However for impedance measurement the PDMS rings would retain PBS (Phosphate-buffered saline) buffer. For the impedance testing the PBS buffer was poured in the MEAs with the PDMS rings and were let to rest for at least 24 hours, ideally 48 hours should be waited with the electrodes soaked in the buffer before testing. This is done to stabilize the electrode-electrolyte interface and avoid hydrophobic interactions that may give values higher than normal impedances. The MEAs were then placed in MEA-IT (Microelectrode Array Impedance Tester) device by Multi Channel Systems, for measurements of electrode impedance, one by one at a time. Figure 8.4 shows the hardware of the MEA-IT device, where the MEA plate is placed in the depression pointed by the red arrow at the base of the device. Once the MEA with the buffer is loaded the top part

of the device is pressed down, the top part of the device has all the amplifier circuitry along with the contact pins shown by the blue arrow that come in contact with the contact pad for the measurements. Once the device is closed and ready for measurement, the operation of the device is done through computer via the interface software that stores the measurement data and helps generate profiles for each MEA accordingly with its data.

The impedance measurements were carried out for all the six prototypes fabricated and for ease of classifying all the six prototypes were given an alphabetic identities, A to F. This was the first time after fabrication they had to be assigned identities so that their corresponding data were storable from this point forth they would be referred by their corresponding alphabetic identity. Amongst all the 6 prototypes, the best measured results were of MEA A, which is shown in figure 8.5 below. The figure of the impedance measurement testing shows the impedance values for each electrode in a specific order that is why it is of prime importance that the MEAs are loaded in a specific order explained in the manual. [15]

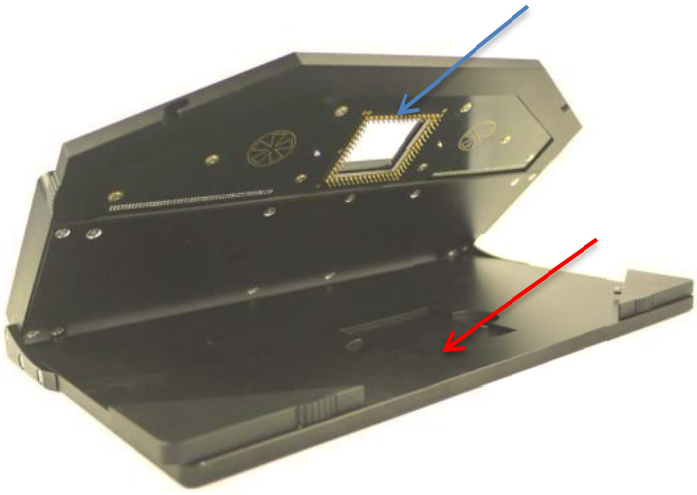

Figure 8.4: *Hardware of the MEA-IT device by Multi Channel Systems, the red arrow shows the MEA plate loading site and the blue arrow shows the contact pins [29]*

The values shown in black, within the grey circles are the impedance values in kilo ohms, the grey circle depict the corresponding electrode and it has its corresponding number in white behind the impedance values. The figure helps understand to relate exactly how, MEA A is best in terms of impedance values and the precision in impedance values as all are below 1200 kΩ.

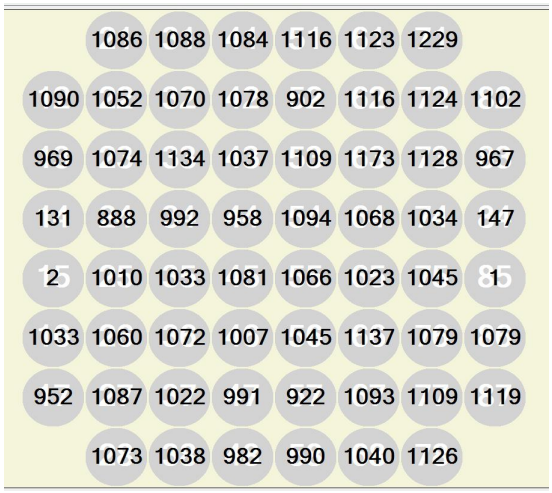

Figure 8.5: *Impedance measurement (in kΩ) of MEA (A) 24 hrs after buffer addition*

From the impedance measurement of each MEA, certain common things can be viewed at once, electrode number 15 and 85 in all MEAs are the reference electrodes and they are much bigger than the rest of the other electrodes. Hence the value of 2 or 1 kΩ, can be seen in figures 8.5 respectively. It can be seen that most values in 'A' range between 888-1228 kΩ. The values of impedance of the electrodes in 'B' were in the range from 700-1459 kΩ. The values of impedance of electrodes in 'C' ranged from 929-1301 kΩ. The values of impedance of electrodes in 'D' ranged from 1011-1359 kΩ. The values of impedance of electrodes in 'E' ranged from 886-1249 kΩ. The values of impedance of electrodes in 'F' range from 1157-1433 kΩ. Though there were also some electrodes in prototypes other than A, with impedances greater than 5000 kΩ, this showed that there was some sort of anomaly in these electrodes. The anomaly could be anything from broken connections in the wiring or narrowing of the connections or defect in the electrode surface etc. An overall average impedance value of the electrodes from all the values were calculated as "1168 kΩ", with a corresponding standard deviation of ±165 kΩ, which did not include values of reference electrodes, or the values above 5000 kΩ as they were considered malfunctioned electrodes.

8.2.2 Noise Measurement Testing

The noise measurement testing was done at BioMediTech, University of Tampere (UTA) with MEA-2100 system by Multi Channel Systems GmbH. The MEA-2100 system was also used for the measurement of the data of beating cardiomyocytes. For the measurement of the noise a similar strategy was assumed where the MEAs were filled up with cell culture media of FBS (Foetal Bovine Serum) and allowed to rest for 24 hours. After 24 hours the MEAs were loaded in the MEA-2100 device and the recordings were made without any cells or contaminations etc. for 90-120 seconds.

Figure 8.6 shows the basic arrangement of a MEA-2100 System for use, thus it should be clear that it requires a good functioning high performance PC. Other than a PC as its

fundamental requirement for operation, the hardware of the MEA-2100 system includes one or two head stages equipped with amplifiers, integrated stimulators and ADCs (Analog to Digital Convertors), and an interface board equipped with an integrated signal processor. The head stage loads the MEAs for measurement and interface board relays the measurement data into digital signal to the computer for display storage and analysis purposes [30].

Figure 8.6: *Fundamental set up of MEA-2100 System in a MEA lab with a PC on the right, Interface board in the middle and 2 Head stages to make MEA recordings [30]*

The noise levels of all the ITO MEA prototypes A-F were measured in comparison to a commercial TiN standard 8 x 8 MEA. The noise levels were measured for each electrode and were stored in a "*.mcd" computer file, which only works with a specific software called "MC_Rack" that interacts with the MEA-2100 system. For analysis the *.mcd file is then converted to a *.txt file using a program called MC_Data Tool which converts the binary data into ASCII code. The *.txt file is then used to import data in forms of vector or matrices for analysis in MATLAB.

Just like all the prototypes were studied for impedance measurements, similarly all the prototypes were tested for noise measurements as well. This would help understand if the impedances of the individual electrodes which were all measured around 1200 kΩ benchmark yielded low noise levels too. Figures 8.7 and 8.8 show the noise measurements of commercial MEA and prototype A in the MC_Rack programme, respectively. Prototype A is chosen to show out of all prototypes here, since it has the best result comparable to the commercial MEA. The figures portray that the noise levels are strikingly similar and comparable, when calculated from a common numbered electrode from both showed that the values were indeed close. The calculated noise voltage for commercial was found to be ± 4.3 μV_{rms} and likewise for prototype A it was ± 7.1 μV_{rms}. However the worst measurement recorded for noise was around 18 μV_{rms}, and the corresponding impedance of the electrode was investigated and found to be 1419 kΩ. A mean noise for all the working electrodes was calculated and found to be 10.67

μV_{RMS} with a standard deviation of ±3.1 µV. This actually shows that the highest noise measurement was sort of an outlier. Nonetheless for 30 µm diameter electrodes the impedance and noise values are more than satisfactory.

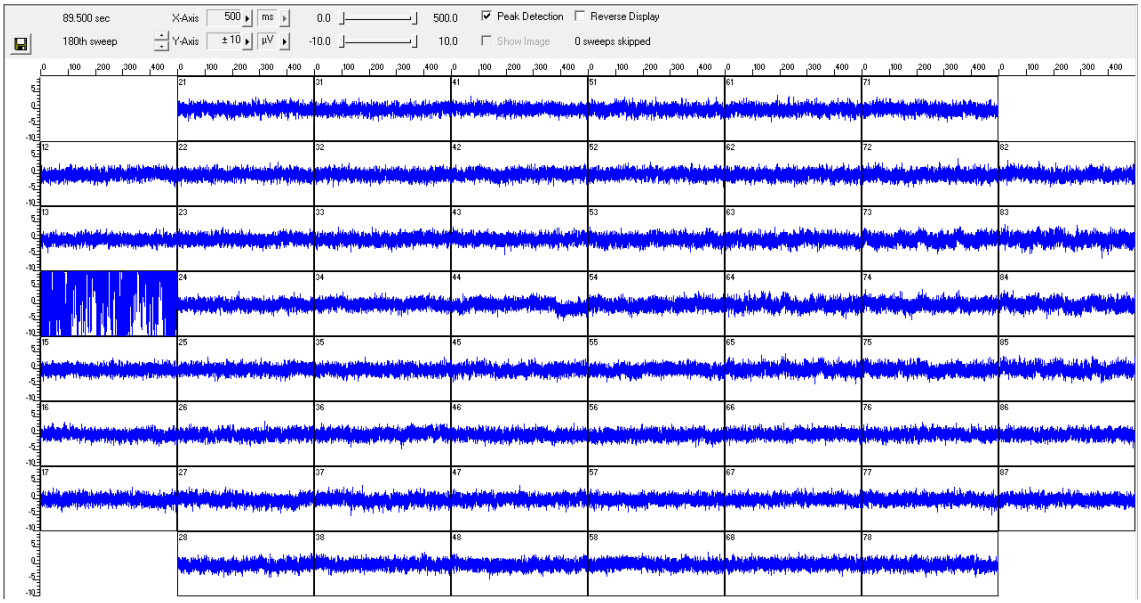

Figure 8.7: *Noise levels of all 60 electrodes from the Commercial TiN MEA in MC_Rack.*

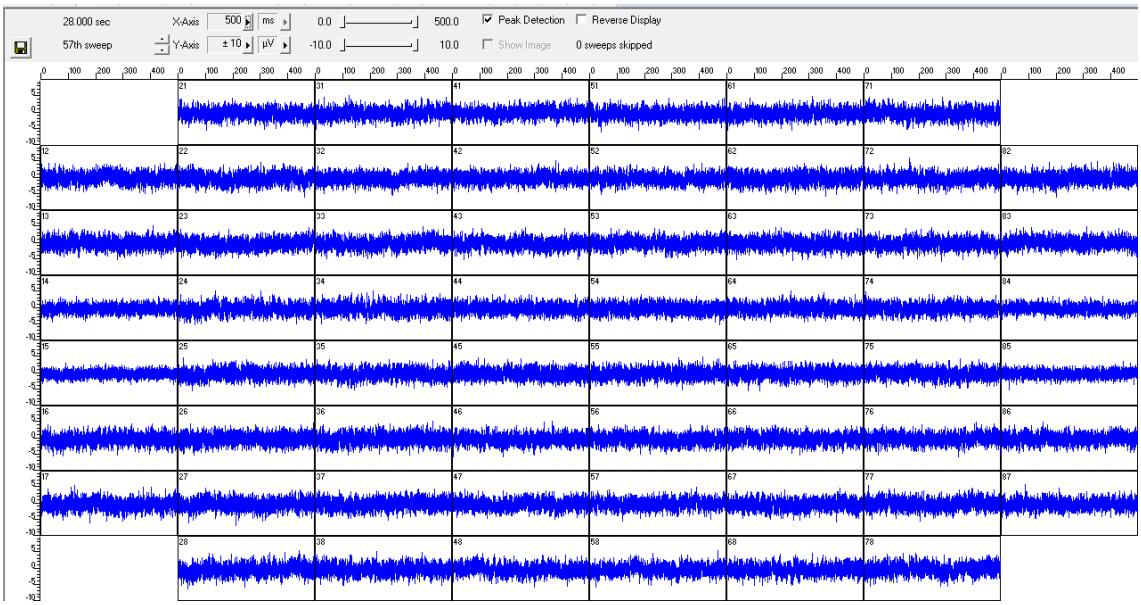

Figure 8.8: *Noise levels of all 60 electrodes from prototype A in MC_Rack.*

8.3 MEA Testing III (Beating Cardiomyocytes)

From the results of the impedance and noise measurements, 2 best specimens were chosen for testing of beating cardiomyocytes, these were prototypes “A” and “C” to be compared with the commercial MEA.

The procedure was similar to the noise measurement, except this time after adding the FBS solution to the sample reservoir in the PDMS rings, slices of beating cardiomyocyte cell aggregates were cultured on top of the electrode region of the MEAs. Once the cell cultures were placed on the electrode regions, a period of waiting followed until the cultures adhered to the electrodes or fixated themselves over the electrodes. This could take from 24 to 72 hours, before a sensible measurement could be made. If the cell cultures did not bind appropriately to the electrodes then on the slightest movement or jerks while moving the MEA chips could cause the culture to float randomly in the reservoir. If the MEAs have temperature sensor in between the electrodes as in the case of this study, then the cultured cells may land on top of the temperature sensor. This may transmit a very faint signal on the neighbouring electrode. Secondly weak adherence of cells also cause technical difficulty in measuring the signal as the magnitude of noise is often comparable with the signals of the cells or the tissue culture. Thus a good binding of the cells to the electrodes determines better results. Figure 8.9 shows the recording of a signal directly from the MC-Rack software of beating cardiomyocytes; here it is evident that the signals magnitude is just slightly higher than the noise.

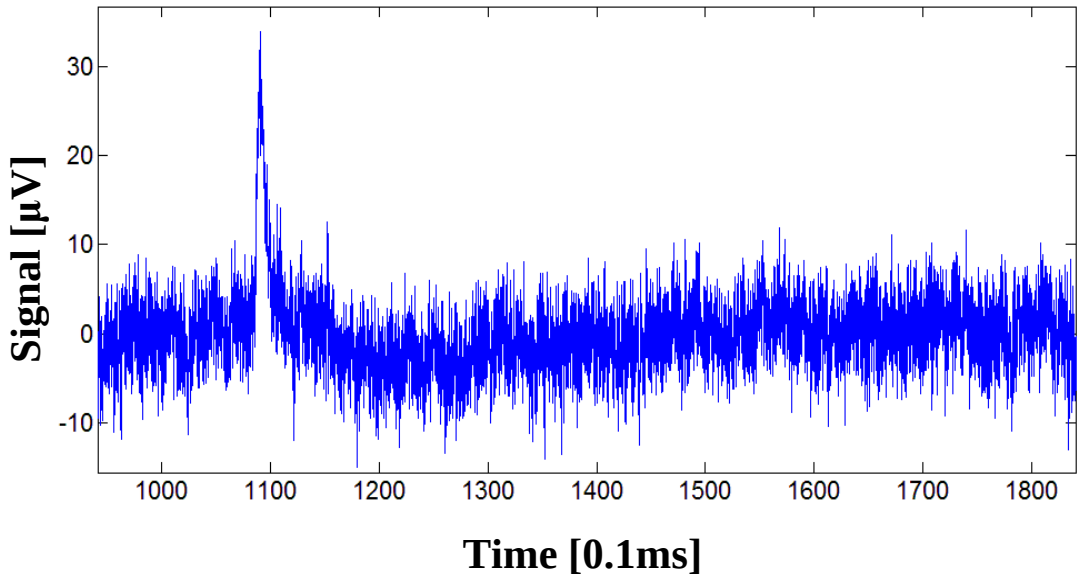

Figure 8.9: *Raw signal recorded directly from MC_Rack of prototype ‘C’.*

The signal attained in Figure 8.9 is then converted into ASCII, as was the case in noise measurements before analysis. This signal is noise prone and using still requires software conditioning to remove the noise and view the actual signal. That all is done via

MATLAB using an in house written program called ‘Cardio MDA’, which accepts the ASCII format text file and subtracts noise signal. The interface of the program takes user inputs as estimates to use averaging techniques and then eliminate the noise. Figure 8.10 shows the corresponding output of the Figure 8.9 after analysis from Cardio MDA program.

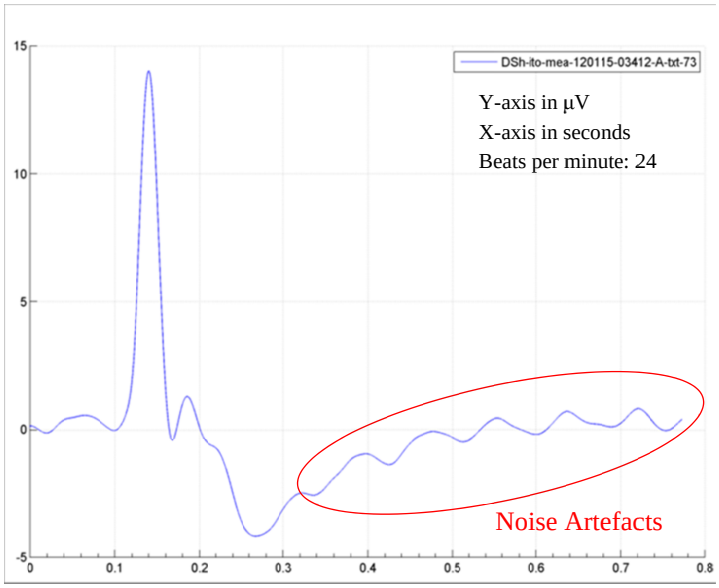

Figure 8.10: *Final result of a beating cardiomyocyte measured by prototype ‘C’ after analysis in Cardio MDA.*

A comparison of final results obtained from Cardio MDA of ‘Commercial TiN’, prototype ‘A’ and prototype ‘C’ can be seen in figure 8.11-8.13 respectively. It can be seen that prototype A and commercial TiN have almost similar results, however prototype C seems to have remnants of noise artefacts even after Cardio MDA analysis which shows that noise levels were high and comparable with signal of the beating cell culture. Figure 8.10 has the similar effects with the wavy parts at the end marked by the red oval.

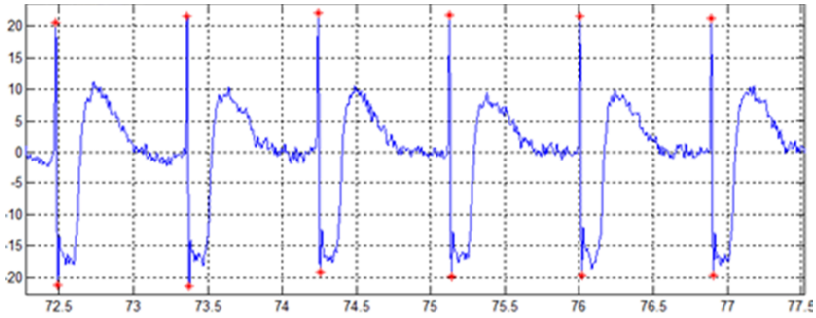

Figure 8.11: *Results measured from a TiN commercial MEA.*

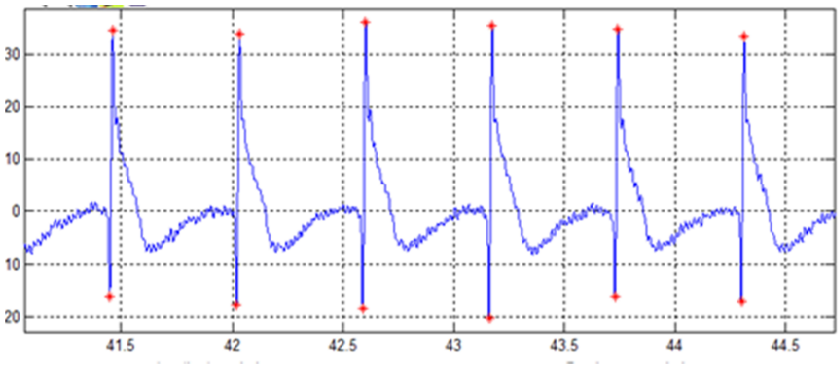

Figure 8.12: *Results measured from prototype 'A' ITO MEA*

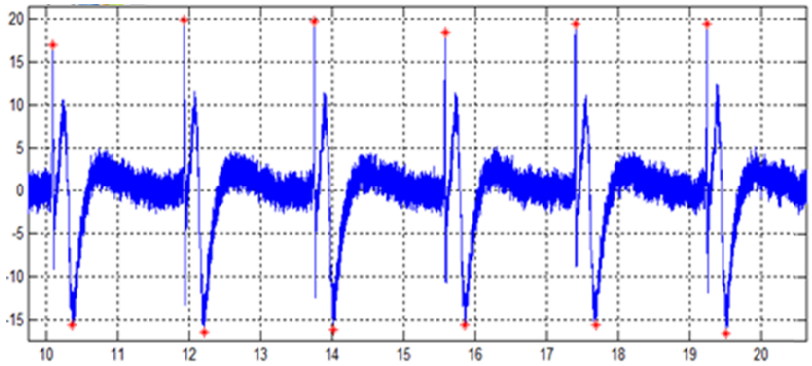

Figure 8.13: *Results measured from prototype 'C' ITO MEA.*

A better understanding of the noise levels and noise artefacts can be seen if single waveform is viewed in a more magnified sense. Thus if figures 8.14-8.16 are reviewed, it can be observed that the least noise artefacts are visible in the TiN commercial MEA. Next to that very little noisy artefacts are barely visible in the prototype A and most noise artefacts are visible in prototype C.

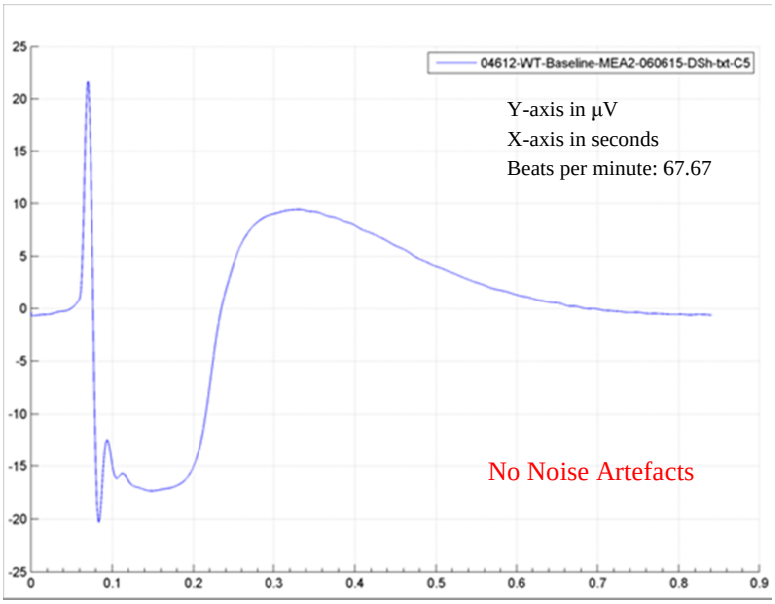

Figure 8.14: *Individual waveform of beating cardiomyocyte from Commercial MEA.*

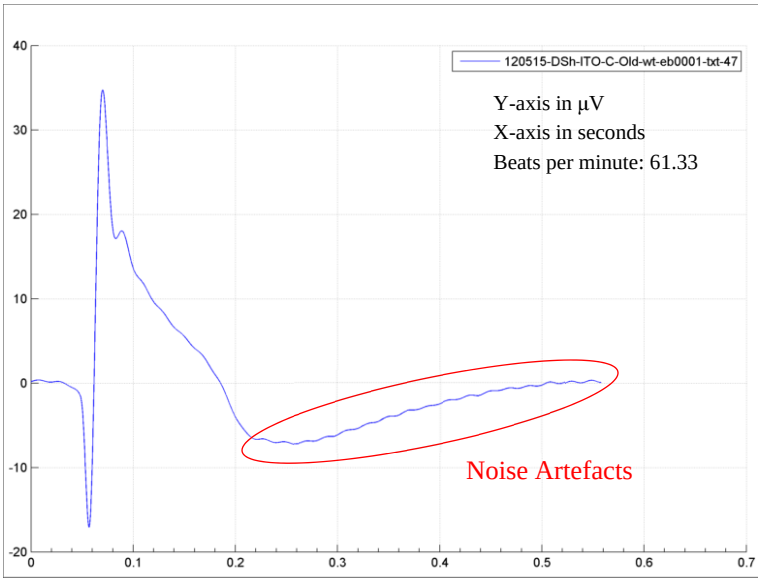

Figure 8.15: *Individual waveform of beating cardiomyocyte from prototype 'A'.*

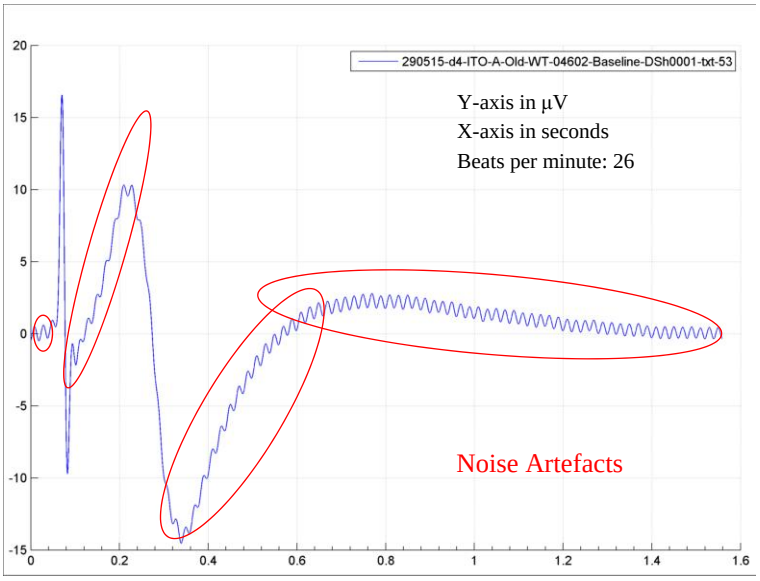

Figure 8.16: *Individual waveform of beating cardiomyocyte from prototype 'C'.*

When comparing Figure 8.15 and Figure 8.16 there is a very distinct understanding of the severe contamination of noise artefacts in prototype C compared to A, there can be more than one explanation for that. The first explanation could be that the noise is innately present due to higher impedance and the particular electrode can be checked for both impedance and noise measurement prior to measurements made. Secondly the noise can also arise from the amplifier system as a result of improper connection of the head stage with the MEA contact pad. For that the head stage could be opened then closed back properly and checked if there are any form of artefacts. Another way to check if the connection pin of the head stage is faulty can be seen by adding a new MEA with only FBS culture medium and make noise measurement afresh. The third reason which occurs the most often is, if the culture temperature decreases due to prolonged measurements the cardiomyocytes beating begin to slow down and the amplitude of the beats recede as well. During this time the beating can become so faint that it begins to match the noise levels more or less. For which the MEA has to be placed back in the culturing incubators for sufficient time so that the cells start to beat between 70-100 bpm again.

In the case of prototype 'C' there were two issues for the presence of higher noise levels resulting in the final output as artefacts. First it can be seen in the diagram the beating rate is mentioned as 26 bpm, second upon referring back to the impedance data of this electrode it was found to be 1301 kΩ which is slightly higher than usual.

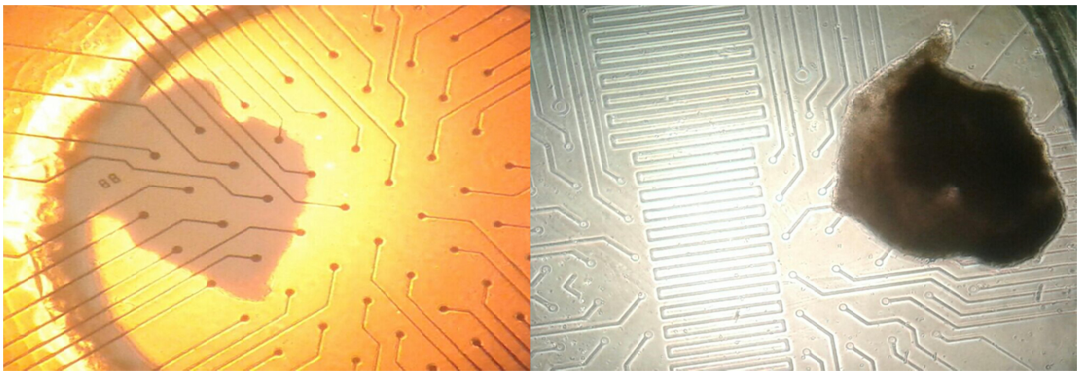

Figure 8.17: *Comparison between Cardiomyocyte aggregate being measured by Commercial TiN MEA (on the right) and by ITO MEA (on the left).*

9. CONCLUSION AND FUTURE PLANS

9.1 Conclusion

9.1.1 Tier I

In this study it is shown that good quality ITO thin layers can be deposited by EB-PVD method over glass substrates, owing to condition that they are subjected to post deposition annealing. The key features that play a vital role in the good quality deposition are low deposition rate of 0.05 nm/s and post annealing of the layer of at temperature ranges between 300-500 °C for no less than an hour. The best result for transparent ITO thin film of 700 μm was achieved at the deposition rate of 0.05 nm/s and post annealing temperature of 300 °C for more than 20 hrs. Though this result was extremely good and much better than reports in [8-10,19,23], but sadly this wasn't utilized for fabricating the MEAs as this result required impractical length of annealing time. Thus the second best result which was observed at 400 °C annealing was utilized as the prime ITO fabrication parameter. Even though the 400 °C 1 hour annealing didn't yield the second best transparency results, but the sheet resistance was best after 300 °C 20 hours process, since lower sheet resistance was preferred over transparency for better quality electrode fabrication thus 400 °C 1 Hour annealing was finalized as the "go-to" process after deposition of ITO as-deposited layers at 0.05 nm/s. The maximum transmittance achieved was 92.8 % and the lowest was 82.3 %, with sheet resistance of 35.8 Ω/sq, which are commercial grade results [31]. Though most commercial ITO layers are not available in thicker layers than 100 nm, yet the layers fabricated in this study have thicknesses up to 700 nm.

9.1.2 Tier II

The best possible quality ITO films were then utilized to microfabricate 8 x 8 Standard MEAs using dry etching with Ar gas (or otherwise known as sputter etching method). The dry etching mechanism was extremely successful in comparison to wet etching using dilute acid solutions, as it provide better controllability and splendid precision in the range of few microns. Though certain references such as [32-34], have reported fabrication of ITO microelectrode using wet etching, however, the experience gained from study contradicts the feasibility of wet etching altogether. The reason for its failure is due to the steeper bias all the etchants owed on to the ITO structures. Similar results were pre authenticated by Shabir et al. in their study as well, whereby small enough geometries experience the etchants to seep under the resist due to isotropic nature of the

etchant [28]. Nevertheless, dry etching is well known for its anisotropic nature and therefore gives a rather precise geometric formulation for magnitude of dimensions below 50 μm in geometry. The study shows that the microfabrication process was successful for microfabrication of MEAs with success to fabrication of a flow sensor with geometric dimensions similar to standard 8 x 8 MEA. The result of the dry etching by the RIE device is not too precise and neither is it a linear process. Due to limitation of time and other unexplored aspects of the study it was decided to utilize the dry etching qualitatively rather than quantitatively. This implies that an etch curve for ITO using sputter etching through RIE wasn't studied. The etching was conducted with basic visual authentication for disappearance of ITO under microscope and by using DMM to check there was no resistance measured on exposed areas luckily, the results were still beyond satisfactory.

9.1.3 Tier III

With success in dry etching to pattern ITO into microstructures and finally as standard 8 x 8 MEAs, the challenges of the study were far from over. Patterning the insulation layer of Si_3N_4 was another mystery that needed solving. The problem was that ITO is a transparent layer and in order to de-insulate the electrodes and the contact pad of the MEAs, the mask for de-insulation couldn't be aligned properly. Thus optimizations were needed to overcome this issue and it was decided to at least have alignment marks that were opaque. For that Ti was chosen to optimize the entire process. A rather odd observation noticed was that though ITO wasn't getting etched as many references have reported, a common etchant that etches ITO etched Ti as well. However, the rate of etching for Ti was extremely faster. The same etchant was expected to etch Ti above ITO as well but that wasn't the case. Ti when deposited on simple glass took mere seconds to etch away 200 nm thick Ti layer, but a similar thick layer over ITO took up to 9 minutes to etch away. Even after the etching the result was devastating, for the underneath ITO layer got destroyed as soon as Ti was all etched away. This had changed the approach so as to now deposit the Ti alignment marks before deposition of ITO altogether. Such an optimization was an inconvenience, nevertheless an absolute necessity as well. The inconvenience was the added labour of an entire layer of fabrication just for adding alignment marks, this increased the time for fabrication by almost 30% and due to addition of an extra layer, process uncertainties rose too. All the necessary labour was applied, so as to produce MEAs which would work. Finally upon the fabrication of successful MEAs, now they had to be tried and tested.

Upon testing it was found that the impedance values of the electrodes were around 1200 kΩ, comparable with commercially available ITO transparent MEAs [35]. Noise levels vary considerably amongst the different prototypes and the reason for that is still unclear. However the best results show very little noise of no more than 7.1 μV_{rms} and the worst results exhibit 18 μV_{rms} levels of noise. Oddly there have been reports of better

and improved electrode impedances such as in [32-33], where they report impedance value slightly above 500 kΩ. Exclusively in one reference it is mentioned that bi layer lift off processed electrodes exhibit impedances at constant 500 kΩ, were as RIE processed ITO electrodes exhibit impedance values vary from 100-3000 kΩ [33]. Though the claimed impedance values are better than the ones presented in this study however, the noise values for the same study are higher than the ones presented in this study. The least noise measure for this study was 7.1 μV_{rms}, the average noise is expected to be 10 μV_{rms} and the highest noise recorded was 18 μV_{rms}. Consequently in [33] ITO's average noise is reported as 14.8 μV_{rms}, whereas gold electrodes noise is reported as 12 μV_{rms} and gold nano particle based electrode exhibits 7.1 μV_{rms}. Clearly the best value of this study and the one being discussed are similar but the point worth considering is that in this study the same noise is being measured from ITO electrode, where as in the other study it is measured from gold nanoparticle electrode. The reduced electrical impedance of an electrode should enable it to achieve higher signal-to-noise ratio values, thus long-term recording, as the noise level is proportional to the electrical impedance [33]. Hence ITO MEAs in this study have earned for themselves a respectable spot as they are comparable to TiN commercial MEAs as demonstrated in Chapter 8 already and the same is true for Au MEAs from [33].

The transparencies of the electrodes show that the cells are completely visible with no obscurities owing to electrodes. The study shows that meaningful data was measured from the MEAs, and that they function as well as any contemporary MEAs (TiN), Au and even other ITO MEAs when compared.

9.2 Future Possibilities

The current progress of this study involves little study for the characterization of the MEAs fabricated. From the study, it is clear that beating cardiomyocytes can be measured using ITO MEAs with electrode diameter as low as 30 μm but could the similar electrodes with smaller diameters be as viable? If so can smaller electrode be designed to an extent that they are able to measure single beating cardiomyocyte at a higher spatial and vectored resolution? What kind of signals will be generated and what will be the challenges in acquiring clear and undistinguishable signals. How much noise will be encountered and how much noise can be attenuated?

Answers to all these questions are yet to be discovered and so it will require surmountable amount of work to figure out if indeed a single cell MEA can be designed using ITO or not. Based on my knowledge from this study I have high hopes that such MEAs can be fabricated using ITO as they have shown promising results for this study. A thorough study for the characterization is still required to measure the different kinds of noise originating from different samples of the same prototypes that were fabricated for this study.

The ITO coating process that was developed for this study was the first of its kind done in our department. Though the quality of the thin films that were deposited wasn't similar to the commercial films available, however it was still comparable. A little more study on the optimization might also prove fruitful in producing better MEAs in future.

Another possibility for future work in transparent MEAs could include testing other TCO such as; AZO (Aluminium doped Zinc Oxide) or FTO (Fluorine doped Tin Oxide) etc. to investigate which thin film yields better MEAs in terms of low noise, high signal, low hysteresis, and are longer lasting. Such a study would prove invaluable in the field of transparent MEAs.

REFERENCES

[1] C. A. Bishop, Vacuum Deposition onto Webs, Films, and Foils, Part 3: Process, Chapter 12: Electron Beam (E-Beam) Evaporation, Elsevier, December 2006, William Andrew, ISBN: 978-0-8155-1535-7.

[2] R.J. Hill, Physical Vapor Deposition, 2nd Edn., Temescal, Berkeley, CA, 1986. Part No. T-0186-6001-1.

[3] Pdf Source: J. Singh, F. Quli, D. E. Wolfe, J. T. Schriempf and J. Singh, "An Overview: Electron Beam-Physical Vapor Deposition Technology- Present and Future Applications"

http://infohouse.p2ric.org/ref/02/01162.pdf, [Last reviewed 5.9. 2015].

[4] D. M. Mattox, Physical Vapor Deposition (PVD) Processing, Surface Engineering, ASM Handbook, Noyes Publications, Westwood, NJ (1998), Vol. 5, ASM International, Materials Park, OH (1994), ISBN 0-8155-1422-0.

[5] Pdf Source: "Transparent Conductive Oxide Thin Films", Technical Paper, Materion Microelectronics & Services, 2978 Main Street, Buffalo, www.materion.com/microelectronics

[6] Web Source: http://en.wikipedia.org/wiki/Indium_tin_oxide [Last reviewed: 15.4.2015].

[7] H. Hosono, H. Ohta, M. Orita, K. Ueda, M. Hirano, Frontier of transparent conductive oxide thin films, Elsevier, Vacuum, August 2002, Volume 66, Issues 3–4, Pages 419-425.

[8] H. R. Fallaha,, M. Ghasemia, A. Hassanzadehb, H. Stekic, The effect of deposition rate on electrical, optical and structural properties of tin-doped indium oxide (ITO) films on glass at low substrate temperature, Elsevier, Physica B, Issue 373 (2006), Pages 274–279.

[9] H. R. Fallaha, , M. Ghasemia, A. Hassanzadehb, H. Stekic, The effect of annealing on structural, electrical and optical properties of nanostructured ITO films prepared by e-beam evaporation, Elsevier, Materials Research Bulletin 42 (2007), Pages 487–496.

[10] H. R. Fallaha, M. Ghasemia, A. Hassanzadehb, Influence of heat treatment on structural, electrical, impedance and optical properties of nanocrystalline ITO films grown on glass at room temperature prepared by electron beam evaporation, Elsevier, Physica E 39 (2007) 69–74.

[11] J. Selvakumaran, M. P. Hughes, J. L. Keddie, D. J. Ewins, Assessing biocompatibility of materials for implantable microelectrodes using cytotoxicity and protein adsorption studies, Annual International IEEE EMBS Special Topic Conference on Microtechnologies in Medicine & Biology, May 24,2002.

[12] I. L. Jones, P. Livi, M. K. Lewandowska, M. Fiscella, B. Roscic, A. Hierlemann, The potential of microelectrode arrays and microelectronics for biomedical research and diagnostics, Analytical and Bioanalytical Chemistry, March 2011, Volume 399, Issue 7, Pages 2313–2329.

[13] M. Fejtl et al. On Micro-Electrode Array Revival: Its Development, Sophistication of Recording, and Stimulation. In: M. Baudry, M. Taketani, eds. Advances in Network Electrophysiology Using Multi-Electrode Arrays. New York: Springer Press; 2006: Pages 24-37.

[14] Multi Channel Sytems Manual 2100 System, Pdf source available at: http://www.multichannelsystems.com/sites/multichannelsystems.com/files/documents/manuals/MEA2100-System_Manual. pdf [last accessed 23. 8.2015].

[15] Multi Channel Sytems MEA Manual, Pdf source available at: http://www.multichannelsystems.com/sites/multichannelsystems.com/files/documents/manuals/MEA_Manual.pdf [last accessed 23. 8.2015].

[16] J.C. Richard. Lithography. Introduction to Microelectronic Fabrication (2nd ed.). Upper Saddle River: Prentice Hall, (2002). ISBN 0-201-44494-1.

[17] Archives on Photolithography from Georgia Tech University, web source: http://www.ece.gatech.edu/research/labs/vc/theory/photolith.html [last accessed 5.9.2015]

[18] Archives on mask types available as product info, web source: http://www.mitani-micro.co.jp/en/mask/photo.html [last accessed 5.11.2016].

[19] J. George, C.S. Menon, “Electrical and optical properties of electron beam evaporated ITO thin films”, Elsevier, Surface and Coatings Technology 2000, Vol.132 Issue 1, Pages 45-48.
.

[20] K. Robbie M. J. Brett. "Sculptured thin films and glancing angle deposition: Growth mechanics and applications." Journal of Vacuum Science & Technology A: Vacuum, Surfaces, and Films 15.3 (1997): Pages 1460-1465.

[21] C. Renault, C. P. Andrieux, R. T. Tucker, M. J. Brett, V. Balland, and B. Limoges, “Unraveling the Mechanism of Catalytic Reduction of O2 by Microp-

eroxidase-11 Adsorbed within a Transparent 3D-Nanoporous ITO Film", Journal of American Chemical Society, 134 (15), pp 6834–6845.

[22] J. G. V. Dijken, M. J. Brett, "Nanopillar ITO electrodes via argon plasma etching", Journal of Vacuum. Science & Technology A 30, 040606 (2012).

[23] J. Zhou, "Indium Tin Oxiide (ITO) Deposition Patterning and Schottky Contact Fabrication", Master's Thesis Study, Department of Microelectronic Engineering, Rochester Institute of Technology, New York 2006.

[24] Archives on product info Menzel glass slides from Thermo Scientific, web sourec: http://www.menzel.de/11-1-Downloads.html. [last accessed 21.11.2016]

[25] C.J. Huang, Y.K. Su, S.L. Wu, "The effect of solvent on the etching of ITO electrode", Elsevier, Materials Chemistry and Physics 84 (2004), Pages146–150

[26] T-H. Tsai, Y-Fu. Wu, "Wet etching mechanisms of ITO films in oxalic acid", Elsevier, Microelectronic Engineering 83 (2006), Pages 536–541.

[27] J-H. Lan, J. Kanicki, A. Catalano, J. Keane, W. D. Boer, T. Gu, "Patterning of transparent conducting oxide thin films by wet etching for a-Si:H TFT-LCDs", Journal of Electronic Materials, December 1996, Volume 25, Issue 12, pp 1806-1817.

[28] S. A. Bashar, "Study of Indium Tin Oxide (ITO) for Novel Optoelectronic Devices", University of London, Ph.D. thesis-Chapter 5, Section 2, Available on: http://www.betelco.com/sb/phd/ch5/c52.html [last accessed 16.9.2015].

[29] Multi Channel Sytems Manual MEA-IT System, Pdf source available at:: http://www.multichannelsystems.com/software/mea-it, "MEA-IT Manual", Multi Channel Systems GmbH: [Last accessed 18.5.2016].

[30] Multi Channel Sytems Manual 2100 System, Pdf source available at:: http://www.multichannelsystems.com/sites/multichannelsystems.com/files/documents/manuals/MEA2100-System_Manual.pdf, [Last accessed 18.5.2016].

[31] Archives on ITO covered glass slides product info from Sigma Aldrich, web Source: http://www.sigmaaldrich.com/catalog/product/aldrich/703184?lang=fi&region=FI&cm_sp=Insite-_-prodRecCold_xviews-_-prodRecCold10-3 [Last accessed 24.11.2016].

[32] Y. Nam, K. Musick & B.C. Wheeler, Application of a PDMS microstencil as a replaceable insulator toward a single-use planar microelectrode array, Kluwer Academic Publishers, Biomedical Microdevices (2006) Volume 8, Issue 4, Pages 375-381.

[33] Y.H. Kim, G.H. Kim, N.S. Baek, Y.H. Han, Ah-Y. Kim, M-Ae. C.S. Jung, Fabrication of multi-electrode array platforms for neuronal interfacing with bi-layer lift-off resist sputter deposition, IOP Publishing Ltd 2013, Journal of Micromechanics and Microengineering, Volume 23, Number 9.

[34] J.V. Pelt, P.S. Wolters, M.A. Corner, W.L.C. Rutten, G.J.A. Ramakers : Long-term characterization of firing dynamics of spontaneous bursts in cultured neural networks. IEEE Trans Biomed Eng. 2004, 51 (11): 2051-2062.

[35] Product catalogue on standard MEA products by Qwane Biosciences SA web source [pdf]: http://www.qwane.com/Documents/Qwane_MEA60_Product_Catalogue_2016.pdf, [Last accessed: 22nd Nov. 2016]

[36] J M Pó, M C Brito, J.M. Alves, J.A. Silva, J.M. Serra, A.M. Vallêra, Measurement of the dopant concentration in a semiconductor using the Seebeck effect, IOP Publishing Ltd 2013, Measurement Science and Technology, Volume 24, Number 5.

APPENDIX: STEP BY STEP MICROFABRICATION PROCESS

1. Cleaning protocol
   - First the glass wafers are immersed in acetone reservoir of the ultrasonic bath for 5 minutes.
   - Then they are ultrasonically cleaned in IPA for 5 minutes.
   - Next they are rinsed with distilled water.
   - Then they are dried off using clean nitrogen blasts
   - Finally the dried glass slides are subjected to oxygen plasma for 5 minutes.

2. E-beam Deposition of Ti film, 200 nm thickness
   - Deposition rate used for Ti is 5 nm/s

3. Cleaning protocol
   - First the glass wafers are immersed in acetone reservoir of the ultrasonic bath for 5 minutes.
   - Then they are ultrasonically cleaned in IPA for 5 minutes.
   - Next they are rinsed with distilled water.
   - Then they are dried off using clean nitrogen blasts

4. Photolithography 1 (for Alignment Marks)
   - First PRI- 2000 A (positive photoresist) is applied to the substrate on the spinner
   - Spin for 45 seconds to 1 minute at 3000 rpm for uniform distribution
   - Substrate is heated at 120°C for 1 minute
   - UV exposure is applied for 25 seconds with mask (mask 1 with alignment marks) for 25 seconds
   - Developed with RD-6 developer for 45 seconds to 1 minute
   - Substrate is heated at 130°C for 1 minute

5. Ti wet etching in 35 % HF+H_2O_2 for 1-2 minutes
   - HF:H_2O_2 (1:10)

6. Stripping Photoresist and Cleaning Protocol
   - First the glass wafers are immersed in acetone reservoir of the ultrasonic bath for 5 minutes.
   - Then they are ultrasonically cleaned in IPA for 5 minutes.
   - Next they are rinsed with distilled water.
   - Then they are dried off using clean nitrogen blasts

7. E-beam Deposition of ITO film, thickness 700 nm
   - ITO used is 90/10 deposition rate of 0.05 nm/s

8. Annealing at 400-450℃ for 1 hour
    - Furnace or a hot plate can be used.

9. Cleaning Protocol
    - First the glass wafers are immersed in acetone reservoir of the ultrasonic bath for 5 minutes.
    - Then they are ultrasonically cleaned in IPA for 5 minutes.
    - Next they are rinsed with distilled water.
    - Then they are dried off using clean nitrogen blasts

10. Photolithography 2 (for ITO Patterning)
    - First PRI- 2000 A is applied to the substrate on the spinner
    - Spin for 45 seconds to 1 minute at 3000 rpm for uniform distribution
    - Substrate is heated at 120°C for 1 minute
    - UV exposure is applied for 25 seconds with mask (mask 2 MEA patterns) for 25 seconds
    - Developed with RD-6 developer for 45 seconds to 1 minute
    - Substrate is heated at 130°C for 1 minute

11. ITO Dry Etching for 80 minutes
    - Sputter etching with RIE device
    - Argon inflow 70 sccm
    - RF- power 250 W
    - Chamber pressure 11 mTorrs

12. Stripping Photoresist and cleaning protocol
    - First the glass wafers are immersed in acetone reservoir of the ultrasonic bath for 5 minutes.
    - Then they are ultrasonically cleaned in IPA for 5 minutes.
    - Next they are rinsed with distilled water.
    - Then they are dried off using clean nitrogen blasts

13. PECVD Deposition of Si_3N_4 (Isolation layer), thickness 500 nm

14. Cleaning Protocol
    - First the glass wafers are immersed in acetone reservoir of the ultrasonic bath for 5 minutes.
    - Then they are ultrasonically cleaned in IPA for 5 minutes.
    - Next they are rinsed with distilled water.
    - Then they are dried off using clean nitrogen blasts

15. Photolithography 3 (for Si_3N_4 Patterning)
    - First PRI- 2000 A is applied to the substrate on the spinner

- Spin for 45 seconds to 1 minute at 3000 rpm for uniform distribution
- Substrate is heated at 120°C for 1 minute
- UV exposure is applied for 25 seconds with mask (mask 3 eith exposed electrodes and contact pads) for 25 seconds
- Developed with RD-6 developer for 45 seconds to 1 minute
- Substrate is heated at 130°C for 1 minute

16. Si_3N_4 Dry Etching for 2.5 minutes
    - RIE device is used with Si_3N_4 $SF_6 + O_2$ etch v1.07 recipe

17. Stripping photoresist and final Cleaning Protocol
    - First the glass wafers are immersed in acetone reservoir of the ultrasonic bath for sufficient time to deserve the resist.
    - Then they are ultrasonically cleaned in IPA for 5 minutes.
    - Next they are rinsed with distilled water.
    - Then they are dried off using clean nitrogen blasts